1 **Title: Mitochondrial respiration contributes to the interferon gamma response in antigen**
2 **presenting cells**
3
4 Short-title: Interferon gamma signaling requires complex I
5

6 Authors: Michael C. Kiritsy[a], Daniel Mott[a], Samuel M. Behar[a], Christopher M. Sassetti[a#],
7 Andrew J. Olive[b#]
8
9
10
11
12 [a]Department of Microbiology and Physiological Systems, University of Massachusetts Medical
13 School, 55 Lake Ave. N, Worcester, Massachusetts 01655, USA.
14
15 [b] Department of Microbiology & Molecular Genetics, Michigan State University, 567 Wilson
16 Road, East Lansing, MI, 48824, USA.
17
18 # Co-corresponding Author
19
20
21 Correspondence:
22
23 Christopher Sassetti
24 christopher.sassetti@umassmed.edu
25 Dept. of Microbiology and Physiological Systems
26 University of Massachusetts Medical School
27 368 Plantation St. ASC8-2051
28 Worcester, MA 01605
29 (508) 856-3678
30
31 Andrew Olive
32 oliveand@msu.edu
33 Department of Microbiology and Molecular Genetics
34 Michigan State University
35 567 Wilson Rd BPS5198
36 East Lansing, MI 48824
37 (517) 884-5367
38
39
40
41

42   **Abstract:**

43

44   The immunological synapse allows antigen presenting cells (APC) to convey a wide array of

45   functionally distinct signals to T cells, which ultimately shape the immune response. The relative

46   effect of stimulatory and inhibitory signals is influenced by the activation state of the APC,

47   which is determined by an interplay between signal transduction and metabolic pathways. While

48   toll-like receptor ligation relies on glycolytic metabolism for the proper expression of

49   inflammatory mediators, little is known about the metabolic dependencies of other critical

50   signals such as interferon gamma (IFNγ). Using CRISPR-Cas9, we performed a series of

51   genome-wide knockout screens in macrophages to identify the regulators of IFNγ-inducible T

52   cell stimulatory or inhibitory proteins MHCII, CD40, and PD-L1. Our multi-screen approach

53   enabled us to identify novel pathways that control these functionally distinct markers. Further

54   integration of these screening data implicated complex I of the mitochondrial respiratory chain in

55   the expression of all three markers, and by extension the IFNγ signaling pathway. We report that

56   the IFNγ response requires mitochondrial respiration, and APCs are unable to activate T cells

57   upon genetic or chemical inhibition of complex I. These findings suggest a dichotomous

58   metabolic dependency between IFNγ and toll-like receptor signaling, implicating mitochondrial

59   function as a fulcrum of innate immunity.

60

61

62

63

64

65 **Introduction:**

66 During the initiation of an adaptive immune response, the antigen presenting cell (APC) serves

67 as an integration point where tissue-derived signals are conveyed to T cells. Myeloid APCs, such

68 as macrophages and dendritic cells (DCs), are responsible for the display of specific peptides in

69 complex with MHC molecules, and for the expression of co-signaling factors that tune the T cell

70 response (1). The expression of stimulatory or inhibitory co-signaling molecules depends on the

71 local immune environment and activation state of the APC (2). In particular, interferon gamma

72 (IFNγ) stimulates the surface expression of MHC proteins (3-9), co-stimulatory proteins such as

73 CD40, and the secretion of cytokines like IL-12 and IL-18 (10), to promote T cell activation and

74 the production of IFNγ-producing T-helper type 1 (Th1) effector cells (11-15). In the context of

75 local inflammation, pattern recognition receptor (PRR) ligands and endogenous immune

76 activators can collaborate with IFNγ to induce the expression of co-inhibitory molecules, like

77 programmed death-ligand 1 (PD-L1) (16-22), which ligates T cell programmed death receptor 1

78 (PD1) to limit immune activation and mitigate T cell-mediated tissue damage (23-26).

79

80 IFNγ mediates these complex effects via binding to a heterodimeric surface receptor (27-

81 30). The subunits of the complex, IFNGR1 and IFNGR2, assemble once IFNGR1 is bound by its

82 ligand (31, 32). Complex assembly promotes the phosphorylation of janus kinases 1 and 2 (JAK1

83 and JAK2) followed by activation of the signal transducer and activation of transcription 1

84 (STAT1) (33). Phosphorylated STAT1 then dimerizes and translocates to the nucleus to activate

85 the transcription of genes containing promoters with IFNγ-activated sequences (GAS), which

86 includes other transcription factors such as interferon regulatory factor 1 (*Irf1*) that amplify the

87 expression of a large regulon that includes T cell co-signaling molecules (34, 35). The

88   importance of this signaling pathway is evident in a variety of diseases including cancer (36-40),

89   autoimmunity (41, 42), and infection (43). Individuals with inborn deficiencies in IFNγ

90   signaling, including mutations to the receptor (44, 45), suffer from a defect in Th1 immunity that

91   results in an immunodeficiency termed Mendelian susceptibility to mycobacterial disease

92   (MSMD) (46-49). Conversely, antagonists of IFNγ-inducible inhibitory molecules, such as PD-

93   L1, are the basis for checkpoint inhibitor therapies that effectively promote T cell-mediated

94   tumor destruction (26, 28, 50-55). While the obligate components of the IFNγ signaling pathway

95   are well known, characterization of additional regulators of this response promises to identify

96   both additional causes of immune dysfunction and new therapeutic targets.

97

98   Recent data suggests that cellular metabolism is an important modulator of the APC-T

99   cell interaction. In particular, microbial stimulation of PRR receptors on the APC induces

100   glycolytic metabolism and this shift in catabolic activity is essential for cellular activation,

101   migration, and CD4+ and CD8+ T cell activation (18, 56-70). The metabolic state of the T cell is

102   also influenced by the local environment and determines both effector function and long-term

103   differentiation into memory cells (71, 72). Like PRR signaling, IFNγ stimulation has been

104   reported to stimulate glycolysis and modulate cellular metabolism in macrophages (66, 73).

105   However, the effects of different metabolic states on IFNγ-stimulated APC function remains

106   unclear.

107

108   To globally understand the cellular pathways that influence IFNγ-dependent APC

109   function, we used a CRISPR-Cas9 knockout library (74) in macrophages to perform a series of

110   parallel forward-genetic screens for regulators of three IFNγ-inducible co-signaling molecules:

111   MHCII, CD40, and PD-L1. We identified positive and negative regulators that controlled each

112   marker, underscoring the complex regulatory networks that influence the interactions between

113   APCs and T cells. Pooled analysis of the screens uncovered shared regulators that contribute to

114   the global IFNγ response. Prominent among these general regulators was complex I of the

115   respiratory chain. We report that the activity of the IFNγ receptor complex and subsequent

116   transcriptional activation depends on mitochondrial function in both mouse and human myeloid

117   cells. Experimental perturbation of respiration inhibits the capacity of both macrophages and

118   dendritic cells to stimulate T cells, identifying mitochondrial function as a central point where

119   local signals are integrated to determine APC function.

120

121   **Results**

122

123   **Forward genetic screen identifies regulators of IFNγ-inducible MHCII, CD40 and PD-L1**

124   **cell surface expression.**

125

126   To investigate the diverse regulatory pathways underlying the IFNγ response, we

127   examined the expression of three functionally distinct cell surface markers that are induced by

128   IFNγ. Stimulation of Cas9-expressing immortalized bone marrow-derived macrophages with

129   IFNγ for 24 hours resulted in the upregulation of T cell stimulatory molecules, major

130   histocompatibility complex class II (MHCII) and CD40, and the inhibitory ligand PD-L1

131   (*Cd274*), on the cell surface (Figure 1A). To identify genes that regulate the expression of these

132   markers, Cas9-expressing macrophages were transduced with a lentiviral genome-wide knockout

133   (KO) library containing four single guide RNAs (sgRNAs) per protein-coding gene and 1000

134   non-targeting control (NTC) sgRNAs (74). The knockout library was then stimulated with IFNγ,

135   and fluorescently activated cell sorting (FACS) was used to select for mutants with high or low

136   cell surface expression of each individual marker (Figure 1B). For each of the three surface

137   markers, positive and negative selections were performed in duplicate. The sgRNAs contained in

138   the input library and each sorted population were amplified and sequenced (Figure 1A,B).

139   To estimate the strength of selection on individual mutant cells, we specifically assessed

140   the relative abundance of cells harboring sgRNAs that target each of the surface markers that

141   were the basis for cell sorting. When the abundances of sgRNAs specific for *H2-Ab1* (encoding

142   the MHCII, H2-I-A beta chain), *Cd40*, or *Cd274* (PD-L1) were compared between high- and

143   low-expressing cell populations, we found that each of these sgRNAs were significantly depleted

144   from the cell populations expressing the targeted surface molecule, while each had no consistent

145   effect on the expression of non-targeted genes (Figure 1C). While not all individual sgRNAs

146   produced an identical effect, we found that targeting the genes that served as the basis of sorting

147   altered the mean relative abundance 30-60 fold, demonstrating that all selections efficiently

148   differentiated responsive from non-responsive cells.

149   We next tested for statistical enrichment of sgRNAs using MAGeCK-MLE (75), which

150   employs a generalized linear model to identify genes, and by extension regulatory mechanisms,

151   controlling the expression of each surface marker. This analysis correctly identified the

152   differential representation of sgRNAs targeting genes for the respective surface marker in the

153   sorted populations in each screen, which were found in the top 20 ranked negative selection

154   scores (Ranks: *H2-Ab1* = 20, *Cd40* = 1, *Cd274* = 3; Table S1). Upon unsupervised clustering of

155   β scores for the most highly enriched genes in each screen (top 5%, positive or negative) both

156   common and pathway-specific effects were apparent (Figure 1D; Table S2). A small number of

157   genes assigned to Cluster 1, including the IFNγ receptor components (*Ifngr1* and *Ifngr2)*, were

158   strongly selected in the non-responsive population in all three selections. However, many

159   mutations appeared to preferentially affect the expression of individual surface markers,

160   including a number of known pathway-specific functions. For example, genes previously shown

161   to specifically control MHCII transcription, such as *Ciita*, *Rfx5*, *Rfxap*, *Rfxank*, and *Creb1* (8, 76-

162   78) were found in Cluster 4 along with several novel regulators that appear to be specifically

163   required for this pathway. MHCII-specific factors are reported in an accompanying study (79).

164   Genes specifically required for CD40 expression in Cluster 3 included the heterodimeric

165   receptor for TNF. *Tnfrsf1a* and *Tnfrsf1b* were the 6th and 50th lowest β scores in the CD40

166   screen, respectively. Previous studies suggested that TNF stimulation enhances IFNγ-mediated

167   CD40 expression in hematopoietic progenitors (80), and we confirmed this observation in

168   macrophages (Figure 1E). We observed a 6-fold higher induction of CD40 in macrophages

169   stimulated with a combination of IFNγ and TNF compared to IFNγ alone. This synergy was

170   specific to CD40 induction, as we did not observe any enhancement of IFNγ-induced MHCII

171   expression by TNF addition.

172   Several recent studies identified genes that control PD-L1 expression in cancer cell

173   lines(28, 53, 55, 81-86), and we validated the PD-L1-associated clusters using these candidates.

174   Our analysis found the previously-described negative regulators, *Irf2* (87), *Keap1*, and *Cul3* (88-

175   90) in the PD-L1-related Cluster 7, along with novel putative negative regulators such as the

176   oligosaccharlytransferase complex subunit *Ostc* and the transcriptional regulator, *Cnbp*. We

177   generated knockout macrophages for each of these novel candidates and confirmed that mutation

178   of these genes enhances the IFNγ-dependent induction of PD-L1 surface levels (Figure 1F).

179 Cumulatively, these data delineate the complex regulatory networks that shape the IFNγ

180 response.

181

182 **Mitochondrial complex I is a positive regulator of the IFNγ response.**

183 To identify global regulators of the IFNγ response, we performed a combined analysis,

184 reasoning that treating each independent selection as a replicate measurement would increase our

185 power to identify novel pathways. We used MAGeCK to calculate a selection coefficient (β) for

186 each gene by maximum likelihood estimation (75). By combining the 24 available measurements

187 for each gene (three different markers, each selection in duplicate, and four sgRNAs per gene),

188 we found that the resulting selection coefficient reflected the global importance of a gene for the

189 IFNγ response (Table S3). The most important positive regulators corresponded to the proximal

190 IFNγ signaling complex (Figure 2A). Similarly, we identified known negative regulators of IFNγ

191 signaling, including the protein inhibitor of activated Stat1 (*Pias1*) (91), protein tyrosine

192 phosphatase non-receptor type 2 (*Ptpn2*) (84), Mitogen activate protein kinase 1 (*Mapk1*), and

193 suppressor of cytokine signaling 1 (*Socs1*) and 3 (*Socs3*).

194 We performed gene set enrichment analysis (GSEA) using a ranked list of positive

195 regulators from the combined analysis (Table S4) (92). Among the top enriched pathways was a

196 gene set associated with type II interferon (e.g., IFNγ) signaling (normalized enrichment score =

197 2.45, q-value = 7.98e-5), validating the approach. GSEA identified a similarly robust enrichment

198 for gene sets related to mitochondrial respiration and oxidative phosphorylation (Figure 2B). In

199 particular, we found a significant enrichment of gene sets dedicated to the assembly and function

200 of the NADH:ubiquinone oxidoreductose (hereafter, "complex I") of the mitochondrial

201 respiratory chain. Complex I couples electron transport with NADH oxidation and is one of four

202 protein complexes that comprise the electron transport chain (ETC) that generates the

203 electrochemical gradient for ATP biosynthesis. To confirm the GSEA results, we examined the

204 combined dataset for individual genes that make up each complex of the ETC (Figure 2C). This

205 analysis demonstrated that sgRNAs targeting components of complexes II, III or IV had minimal

206 effects on the expression of the IFNγ-inducible surface markers tested. In contrast, the disruption

207 of almost every subunit of complex I impaired the response to IFNγ, with the notable exception

208 of *Ndufab1*. As this gene is essential for viability (93), we assume that cells carrying *Ndufab1*

209 sgRNAs retain functional target protein.

210   To investigate the contribution of specific complex I components to different IFNγ-

211 stimulated phenotypes, we reviewed the surface marker-specific enrichment scores for genes that

212 contribute to the complex assembly, the electron-accepting N-module, or the electron-donating Q

213 module (93-98). Of the 48 individual assembly factors or structural subunits of complex I present

214 in our mutant library, 29 were significantly enriched as positive regulators in the global analysis

215 and were generally required for the induction of all IFNγ-inducible markers (Fig. 2D). The

216 enrichment for each functional module in non-responsive cells was statistically significant.

217 However, not all individual complex I components were equally enriched, which could reflect

218 either differential editing efficiency or distinct impacts on function. To investigate the latter

219 hypothesis, we compared our genetic data with a previous proteomic study that quantified the

220 effect of individual complex I subunits on the stability of the largest subcomplex, the N-module

221 (93). For a given subunit, we found a significant correlation between the magnitude of

222 enrichment in our genetic screen and its effect on the structural stability of the module (Fig. 2E),

223 specifically implicating the activity of complex I in the IFNγ response.

224   To directly test the predictions of the screening data, we used CRISPR to generate

225   individual macrophage lines that were deficient for complex I subunits. We first validated the

226   expected metabolic effects of complex I disruption by comparing the intracellular ATP levels in

227   macrophages carrying non-targeting control sgRNA (sgNTC) with sg*Ndufa1* and sg*Ndufa2* lines.

228   When cultured in media containing the glycolytic substrate, glucose, all cell lines produced

229   equivalent amounts of ATP (Figure 3A). However, when pyruvate was provided as the sole

230   carbon source, and ATP generation depends entirely upon flux through ETC and oxidative

231   phosphorylation (OXPHOS), both sg*Ndufa1* and sg*Ndufa2* macrophages contained decreased

232   ATP levels compared to sgNTC cells (Figure 3B). To confirm the glycolytic dependency of

233   complex I mutant macrophages, we grew cells in complete media with glucose and treated with

234   the ATP synthase (complex V) inhibitor, oligomycin, which blocks ATP generation by

235   OXPHOS. While oligomycin reduced ATP levels in sgNTC macrophages, this treatment had no

236   effect in sg*Ndufa1* and sg*Ndufa2* cells (Supplementary Figure 1A), confirming that these

237   complex I-deficient cells rely on glycolysis for energy generation. IFNγ treatment slightly

238   reduced ATP levels in glucose containing media but did not differentially affect cell lines (Figure

239   3A). Throughout these experiments we found that the sg*Ndufa1* mutant showed a greater

240   OXPHOS deficiency than the sg*Ndufa2* line.

241   We next compared the response to IFNγ in macrophages lacking *Ndufa1* and *Ndufa2* with

242   those carrying CRISPR-edited alleles of *Ifngr1* or the negative regulator of signaling, *Ptpn2*. As

243   CD40 was found to rely on more complex inputs for expression, which include TNF (Figure 1E),

244   we relied on MHCII and PD-L1 as markers of the IFNγ response for subsequent studies. As

245   expected, and consistent with the genetic screen, we found that the loss of *Ifngr1* or *Ptpn2* either

246   abrogated or enhanced the response to IFNγ, respectively. Also consistent with predictions,

247 mutation of complex I genes significantly reduced the IFNγ-dependent induction of MHCII and

248 PD-L1 compared to sgNTC (Figure 3C-F). The *Ndufa1* mutation that abrogates OXPHOS,

249 reduced MHCII induction to the same level as *Ifngr1*-deficient cells. To confirm these results

250 using an orthologous method we treated cells with the complex I inhibitor, rotenone (99). This

251 treatment caused a dose-dependent inhibition of the IFNγ-induced MHCII expression in sgNTC

252 macrophages (Figure 3G) and had a similar inhibitory effect on the residual IFNγ response in

253 *Ndufa2*-deficient cells. Together these results confirm that complex I is required for the induction

254 of immunomodulatory surface molecules in response to IFNγ.

255   To investigate what aspect of mitochondrial respiration contributes to the IFNγ response,

256 we inhibited different components of the ETC. All inhibitors were used at a concentration that

257 abrogated OXPHOS-dependent ATP generation (Supplementary Figure 1B). The complex V

258 inhibitor, oligomycin, inhibited the IFNγ-induced MHCII expression, albeit to a lesser extent

259 than direct complex I inhibition with rotenone (Figure 3H). This partial effect could reflect an

260 inability to dissipate the proton motive force (PMF), which inhibits electron flux throughout the

261 ETC, including through complex I (100). Carbonyl cyanide m-chlorophenyl hydrazone (CCCP)

262 disrupts mitochondrial membrane potential and OXPHOS while preserving electron flux. CCCP

263 had no effect on the IFNγ response, indicating that ATP generation is dispensable for

264 IFNγ responsiveness and highlighting a specific role for complex I activity.

265   We then altered the media composition to test the sufficiency of mitochondrial respiration

266 to drive IFNγ responses independently from aerobic glycolysis. IFNγ was found to stimulate

267 MHCII expression to a similar degree in macrophages cultured in complete media with glucose

268 as in media containing only pyruvate or citrate, which must be catabolized via mitochondrial

269 respiration (Figure 3H). Inhibition of mitochondrial pyruvate import with the chemical inhibitor,

270   UK5099 (101), abrogated MHCII induction in cultures grown in pyruvate, but not in citrate,

271   which is imported via a UK5099-independent mechanism. Taken together these results suggest

272   that cellular respiration is both necessary and sufficient for maximal expression of the IFNγ-

273   inducible surface markers MHCII and PD-L1.

274

275   **Mitochondrial function is specifically required IFNγ-dependent responses.**

276   The mitochondrial-dependency of the IFNγ response contrasted with the known

277   glycolytic-dependency of Toll-like receptor (TLR) signaling, suggesting that TLR responses

278   would remain intact when complex I was inhibited. Indeed, not only were TLR responses intact

279   in sg*Ndufa1* and sg*Ndufa2* mutant macrophages, these cells secreted larger amounts of TNF or

280   IL-6 than sgNTC cells in response to the TLR2 ligand, Pam3CSK4. (Figure 4A). Thus, the

281   glycolytic dependency of these cells enhanced the TLR2 response, indicating opposing metabolic

282   dependencies for IFNγ and TLR signaling.

283   Whether the effects of complex I on macrophage responsiveness was the result of

284   reduced mitochondrial respiratory function or secondary to cellular stress responses, such as

285   radical generation, remained unclear. To more directly relate mitochondrial function to these

286   signaling pathways, we created cell lines with reduced mitochondrial mass. Macrophages were

287   continuously cultured in linezolid (LZD), an oxazolidinone antibiotic that inhibits the

288   mitochondrial ribosome (102-104). This treatment produced a cell line with ~50% fewer

289   mitochondrial genomes per nuclear genome and a corresponding decrease in OXPHOS capacity,

290   compared to control cells grown in the absence of LZD (Figure 4B,C). Cells were cultured

291   without LZD for 16 hours and then stimulated with either IFNγ or Pam3CSK4. Consistent with

292   our complex I inhibition studies, we found this reduction in mitochondrial mass nearly abrogated

293   the IFNγ-dependent induction of MHCII (Figure 4D), while the TLR2-dependent secretion of

294   TNF and IL-6 was preserved or enhanced (Figure 4E and 4F). Thus, mitochondrial activity,

295   itself, is necessary for a robust IFNγ response.

296   To further address potential secondary effects of mitochondrial inhibition on the

297   IFNγ response, we investigated the role of known oxygen or nitrogen radical-dependent

298   regulators (Supplementary Figure 1C-G). Inhibition of ROS generation by replacing glucose

299   with galactose (66, 100, 105) had no effect on IFNγ-induced MHCII induction. Similarly,

300   neutralization of cytosolic or mitochondrial radicals with N-acetylcysteine or MitoTempo,

301   respectively, had no effect on MHCII induction either alone or in combination with ETC

302   inhibition. The role of the cytosolic redox sensor, $HIF1\alpha$ (106, 107) was addressed by

303   chemically stabilizing this factor with dimethyloxalylglycine (DMOG). A potential role for nitric

304   oxide production was addressed with the specific NOS2 inhibitor 1400W (60, 66, 108). Neither

305   of these treatments affected IFNγ-induced MHCII cell surface expression in the presence or

306   absence of simultaneous Pam3CSK4, further supporting a direct relationship between

307   mitochondrial respiratory capacity and the IFNγ response.

308

309   **Complex I is specifically required for IFNγ signaling in human cells.**

310   To understand the function of complex I during IFNγ-stimulation in human cells, we used

311   monocyte-derived macrophages (MDM) from peripheral blood of healthy donors. As in our

312   mouse studies, we assessed the response of these cells to IFNγ or Pam3CSK4 by quantifying the

313   abundance of IFNγ-inducible surface markers or cytokines that were optimized for human cells.

314   Since HLA-DR is not strongly induced by IFNγ, we included ICAM1 in addition to CD40 and

315   PD-L1 as surface markers. As seen in the murine model, rotenone inhibited the IFNγ-mediated

316   induction of all three markers (Figure 5A). TLR2 responses were assessed by the production of

317   TNF and IL-1β. Upon Pam3CSK4 stimulation, rotenone significantly enhanced the secretion of

318   IL-1β and TNF (Figure 5B). While simultaneous treatment with both IFNγ and Pam3CSK4

319   produced the previously described inhibition of IL-1β (109), rotenone still did not decrease the

320   production of these TLR2 dependent cytokines. Thus, as we observed in mouse cells, complex I

321   is specifically required for IFNγ signaling in human macrophages.

322

323   **Complex I inhibition reduces IFNγ receptor activity.**

324   To understand how complex I activity was shaping the IFNγ response, we first

325   determined whether its effect was transcriptional or post-transcriptional by simultaneously

326   monitoring mRNA and protein abundance over time. Surface expression of PD-L1 was

327   compared with the gene's mRNA abundance, while the surface expression of MHCII was

328   compared with the mRNA abundance of *Ciita*, the activator of MHCII expression that is initially

329   induced by IFNγ (Figure 6 A,B). In both cases, mRNA induction preceded surface expression of

330   the respective protein. More importantly, both mRNA and protein expression of each marker was

331   diminished to a similar degree in sg*Ndufa1* and sg*Ndufa2*, compared to sgNTC cells. Thus, a

332   deficit in transcriptional induction could account for the subsequent decrease in surface

333   expression observed in complex I deficient cells.

334   IFNγ rapidly induces the transcription of a large number of STAT1 target genes,

335   including IRF1, which amplifies the response. The relative impact of complex I inhibition on the

336   immediate transcriptional response versus the subsequent IRF1-dependent amplification was

337   initially assessed by altering the timing of complex I inhibition. As the addition of rotenone was

338   delayed relative to IFNγ stimulation, the ultimate effect on MHCII expression was diminished

339   (Figure 6C). If rotenone was added more than 4 hours after IFNγ, negligible inhibition was

340   observed by 24 hours, indicating that early events were preferentially impacted by rotenone. To

341   more formally test the role of IRF1, this study was performed in macrophages harboring a

342   CRISPR-edited *Irf1* gene. While the level of MHCII induction was reduced in the absence of

343   IRF1, the relative effect of rotenone addition over time was nearly identical in sg*Irf1* and sgNTC

344   cells. Thus, mitochondrial function appeared to preferentially impact the initial transcriptional

345   response to IFNγ upstream of IRF1.

346   Ligand induced assembly of the IFNGR1-IFNGR2 receptor complex results in the

347   phosphorylation and transactivation of janus kinases 1 and 2 (JAK1, JAK2).

348   Autophosphorylation of JAK2 at tyrosine residues 1007/1008 positively regulates this cascade

349   and serves as a marker of JAK2 activation. These activating events at the cytoplasmic domains

350   of the IFNGR receptor complex facilitate STAT1 docking and phosphorylation at tyrsone-701

351   (Y701), a prerequisite for the IFNγ response. Additional STAT1 phosphorylation at serine-727

352   can amplify signaling. To determine if complex I is required for these early signal transduction

353   events, we examined the activation kinetics by immunoblot (Figure 6D). The total abundances of

354   IFNGR1, STAT1, and JAK2, were constant in sgNTC and sg*Ndufa1* cells in the presence and

355   absence IFNγ-stimulation. While we detected robust phosphorylation of JAK2 Y1007/8, STAT1-

356   Y701, and STAT1-S727 over time following IFNγ treatment in sgNTC cells, phosphorylation at

357   all three sites was both delayed and reduced across the time-course in sg*Ndufa1* cells. We

358   conclude that the loss of complex I function inhibits receptor proximal signal transduction

359   events.

360

361 **Mitochondrial respiration in antigen presenting cells is required IFNγ-dependent T cell**

362 **activation.**

363   As respiration affected both stimulatory and inhibitory antigen presenting cell (APC)

364 functions, we sought to understand the ultimate effect of mitochondrial function on T cell

365 activation. To this end, we generated myeloid progenitor cell lines from Cas9-expressing

366 transgenic mice that can be used for genome-edited and differentiated into either macrophages or

367 dendritic cells using M-CSF or FLT3L, respectively (110, 111). Macrophages differentiated from

368 these myeloid progenitors demonstrated robust induction of all three markers that were the basis

369 for the IFNγ stimulation screens (Supplementary Figure 2A-C). Further, both the IFNγ-mediated

370 upregulation of these markers and the inhibitory effect of rotenone or oligomycin on their

371 induction were indistinguishable from wild-type primary bone marrow-derived macrophages

372 (Supplementary Figure 2D-F). In both macrophages and in dendritic cells (DCs), the induction of

373 MHCII by IFNγ was inhibited by rotenone and oligomycin (Figure 7A). Unlike macrophages,

374 murine DCs basally express MHCII and these inhibitors only repressed the further induction by

375 IFNγ (Figure 7A,B).

376   Both macrophages and DCs were used to determine if the inhibition of complex I in

377 APCs reduces T cell activation. Both types of APCs were stimulated with IFNγ overnight with or

378 without rotenone before washing cells to remove rotenone and ensure T cell metabolism was

379 unperturbed. APCs were then pulsed with a peptide derived from the *Mycobacterium*

380 *tuberculosis* protein ESAT-6, and co-cultured with ESAT-6-specific CD4+ T cells from a TCR

381 transgenic mouse (112). T cell activation was assayed by intracellular cytokine staining for IFNγ.

382 In macrophages, T cell stimulation relied on pretreatment of the APC with IFNγ, as a

383   macrophage line lacking the *Ifngr1* gene was unable to support T cell activation. Similarly,

384   inhibition of complex I in macrophages completely abolished antigen-specific T cell stimulation

385   (Figure 7C). DCs did not absolutely require IFNγ pretreatment to stimulate T cells, likely due to

386   the basal expression of MHCII by these cells. Regardless, rotenone treatment of DC abrogated

387   the IFNγ-dependent increase in T cell stimulation (Figure 7C).

388   To confirm the effects of complex I inhibition on T cell activation using a genetic

389   approach and confirm that complex I inhibition acted in a cell-autonomous mechanism, we

390   generated *Ndufa1* knockout myeloid progenitors (Hox-sg*Ndufa1*). Following differentiation into

391   macrophages, Hox-sg*Ndufa1* demonstrated glycolytic dependence and the inability to generate

392   ATP by OXPHOS compared to control Hox-sgNTC macrophages (Supplementary Figure 2G).

393   Having confirmed the expected metabolic effects of Ndufa1 loss, Hox-sg*Ndufa1* and Hox-

394   sgNTC macrophages were mixed at various ratios. Mixed cultures were then stimulated with

395   IFNγ, peptide pulsed, and co-cultured with antigen-specific CD4+ T cells. In agreement with our

396   chemical inhibition studies, we found strong correlation between complex I activity in the APC

397   population and T cell stimulatory activity (Figure 7D-E). Together, these data confirm that the

398   IFNγ-dependent augmentation of T cell stimulatory activity depends on complex I function in

399   both macrophages and DCs.

400

401   **Discussion**

402   IFNγ-mediated control of APC function is central to shaping a protective immune

403   response, and the canonical IFNγ signal transduction pathway has been elucidated in exquisite

404   detail (113). Our study demonstrates that unbiased genetic analyses can reveal a multitude of

405   unexpected cellular regulators, even for a well-characterized process such as IFNγ signaling. By

406   independently assessing genetic determinants of stimulatory and inhibitory molecule expression,

407   we discovered mechanisms of regulation that preferentially affect the induction of different cell

408   surface proteins. These results begin to explain how a single cytokine can induce functionally

409   distinct downstream responses in different contexts. These data also suggest new strategies to

410   modulate individual co-receptors to either stimulate or inhibit T cell activation. Another strength

411   of our parallel screen approach was the increased power to identify shared mechanisms that

412   control IFNγ-mediated regulation across all screens. Our pooled analysis identified

413   mitochondrial respiration, and in particular complex I, as essential for IFNγ-responses in APCs.

414   We determined that complex I is required for the IFNγ-mediated induction of key immune

415   molecules and is necessary for antigen presentation and T cell activation. These findings uncover

416   a new dependency between cellular metabolism and the immune response.

417   Our genetic and chemical inhibition data demonstrated that mitochondrial respiration is

418   necessary for early events in signal transduction from the IFNγ receptor complex, and complex I

419   of the respiratory chain is specifically required. While IFNγ stimulation has been reported to

420   mediate a reduction in oxygen consumption and a shift to aerobic glycolysis over time (66), the

421   requirement of mitochondrial respiration in IFNγ responses has not been assessed previously.

422   Our results indicate that complex I is required for IFNγ signaling regardless of these metabolic

423   shifts. Complex I is a metabolic hub with several core functions that cumulatively recycle

424   nicotinamide adenine dinucleotide (NAD+), reduce ubiquinol, and initiate the PMF for ATP

425   generation. While any or all of these physiologic processes could contribute to IFNγ signaling,

426   the differential effects of chemical inhibitors narrow the possibilities. Both rotenone and

427   oligomycin inhibit the IFNγ response, and block electron flux through complex I either directly

428   or indirectly. In contrast, the ionophore CCCP disrupts the PMF and ATP generation without

429   inhibiting electron transfer, and does not affect IFNγ signaling. These data indicate that the

430   reduction state of the quinone pool and ATP generation do not regulate IFNγ responses in our

431   system. Instead, complex I-dependent regeneration of NAD+ is the most likely regulator of IFNγ

432   signaling. Indeed, NAD+ synthesis via either the *de novo* or salvage pathway is necessary for a

433   variety of macrophage functions (114-116). Very recent work demonstrates an important role for

434   NAD+ in STAT1 activation and PD-L1 induction by IFNγ in hepatocellular carcinoma cells

435   (117). In this setting, inhibition of NAD+ synthesis reduces the abundance of phospho-STAT1

436   by disrupting a direct interaction with the Ten-eleven translocation methylcytosine dioxygenase

437   1 (TET1). It remains unclear if a similar interaction occurs in the myeloid cells that are the focus

438   of our work, as TET1 is expressed at very low levels in macrophages and splenic DC (118).

439   Regardless, these observations indicate that both NAD+ synthesis and its regeneration via

440   mitochondrial respiration contribute to the IFNγ response in diverse cell types. This recently

441   revealed interaction between metabolism and immunity could contribute to the observed

442   association between NAD+ homeostasis and inflammatory diseases (116), as well as the efficacy

443   of checkpoint inhibitor therapy for cancer (117).

444   In the APC setting, we found that T cell activation required mitochondrial respiration.

445   While complex I function, MHCII and CD40 expression all largely correlate with T cell

446   stimulation, our data indicate that additional IFNγ-inducible pathways also contribute to this

447   activity. For example, unstimulated DCs basally express similar levels of MHCII as IFNγ-

448   stimulated macrophages but are unable to productively present antigen to T cells. This

449   observation suggests that additional aspects of antigen processing, presentation, or co-stimulation

450   are IFNγ- and complex I-dependent. Similarly, MHCI presentation machinery is transcriptionally

451   induced upon IFNγ stimulation (7, 119) and the induction of molecules recognized by donor

452   unrestricted T cells, such as MR1 and CD1, might also require additional signals to function. The

453   specific effects of mitochondrial respiration on the type and quality of the T cell response will

454   depend on how these diverse antigen-presenting and co-signaling molecules are influenced by

455   cellular metabolic state.

456   The observation that IFNγ signaling depends on mitochondrial respiration provides a

457   stark contrast to the well-established glycolytic dependency of many phagocyte functions, such

458   as TLR signaling. This metabolic dichotomy between proinflammatory TLR signals and the

459   IFNγ response mirrors known regulatory interactions between these pathways. For example,

460   TLR stimulation has been shown to inhibit subsequent IFNγ responses, via a number of target

461   gene-specific mechanisms (120-124). However, TLR stimulation also results in the disassembly

462   of the ETC (123, 124), which our observations predict to inhibit STAT1 phosphorylation and

463   IFNγ signaling at the level of the receptor complex. More generally, our work suggests

464   fundamental metabolic programs contribute to the integration of activation signals by APC and

465   influence the ultimate priming of an immune response.

466

467   **Materials and Methods**

468   **Cell culture**

469   Cells were cultured in Dulbecco's Modified Eagle Medium (Gibco 11965118) supplemented

470   with 10% fetal bovine serum (Sigma F4135), sodium pyruvate (Gibco 11360119), and HEPES

471   (15630080). Primary bone marrow-derived macrophages (BMDMs) were generated by culturing

472   bone marrow in the presence of media supplemented with 20% L929 supernatant for 7 days.

473

474   Immortalized macrophage cell lines in C57Bl6/J and Cas9-EGFP were established in using J2

475   retrovirus from supernatant of CREJ2 cells as previously described(125). Briefly, isolated bone

476   marrow was cultured in the presence of media enriched with 20% L929 supernatant. On day 3,

477   Cells were transduced with virus and cultured with virus for 2 days. Over the next 8 weeks, L929

478   media was gradually reduced to establish growth factor independence.

479

480   Conditionally immortalized myeloid progenitor cell lines were generated by retroviral

481   transduction using an estrogen-dependent Hoxb8 transgene as previously described(110).

482   Briefly, mononuclear cells were purified from murine bone marrow using Ficoll-Paque Plus (GE

483   Healthcare 17144002) and cultured in RPMI (Gibco 11875119) containing 10% fetal bovine

484   serum (Sigma F4135), sodium pyruvate (Gibco 11360119), and HEPES (15630080), IL-6

485   (10ng/mL; Peprotech #216-16), IL-3 (10ng/mL; Peprotech #213-13), and SCF (10ng/mL;

486   Peprotech #250-03) for 48 hours. Non-adherent bone marrow cells from C57Bl6/J (Jax 000664),

487   Cas9-EGFP knockin (Jax 026179), or Ifngr1 knockout (Jax 003288) mice were transduced with

488   ER-Hoxb8 retrovirus. After transduction cells were cultured in with media supplemented with

489   supernatant from B16 cells expressing GM-CSF and 10uM estradiol (Sigma E8875) to generate

490   macrophage progenitor cell lines or in media supplemented with supernatant from B16 cells

491   expressing FLT3L and 10uM estradiol (Sigma E8875) to generate dendritic cell progenitor lines.

492   To differentiate macrophages, progenitors were harvested and washed twice with PBS to remove

493   residual estradiol and cultured in L929 supplemented media as above. To differentiate dendritic

494   cells(111), progenitors were harvested, washed 2x with PBS, and cultured in FLT3-enriched

495   complete RPMI for 8-10 days.

496

497   Human monocyte-derived macrophages (MDM) were differentiated from mononuclear cells of

498   healthy donors. Briefly, peripheral blood mononuclear cells (PBMCs) were isolated from whole

499   blood using Ficoll-Paque-PLUS (GE Healthcare 17144002). CD14+ monocytes were purified

500   using MojoSort™ Human CD14 Nanobeads (Biolegend 480093) according to the manufacturer's

501   protocol. Cells were cultured in RPMI with 10% FBS, sodium pyruvate, and HEPES and

502   supplemented with recombinant GM-CSF (50ng/mL, Peprotech 300-03) for 6 days. Thaws were

503   harvested using Accutase (Gibco A1110501).

504

505   **Cell stimulations**

506   Murine IFNγ (Peprotech 315-05) and human IFNγ (Peprotech 300-02) were used at 10ng/mL

507   unless otherwise indicated in the figure legends. Murine TNF (315-01A) was used at 25ng/mL.

508   Pam3CSK4 (Invivogen tlrl-pms) was used at 200ng/mL.

509

510   **CRISPR screens**

511   A clonal macrophage cell line stably expressing Cas9 (L3) was established as described

512   elsewhere(79). A plasmid library of sgRNAs targeting all protein coding genes in the mouse

513   genome (Brie Knockout library, Addgene 73633) was packaged into lentivirus using HEK293T

514   cells. HEK293T supernatants were collected and clarified, and virus was titered by quantitative

515   real-time PCR and by colony counting after transduction of NIH3T3. L3 cells were transduced at

516   a multiplicity of infection (MOI) of ~0.2 and selected with puromycin 48 hours after

517   transduction (2.5ug/mL). The library was minimally expanded to avoid skewing mutant

518   representation and then frozen in aliquots in freezing media (90% FBS 10% DMSO).

519

520   Two replicate screens for MHCII, CD40, and PD-L1 were performed as follows:

521   2e8 cells of the knockout (KO) library was stimulated with IFNγ (10ng/mL; Peprotech 315-05)

522   for 24 hours after which cells were harvested by scraping to ensure integrity of cell surface

523   proteins. Cell were stained with TruStain FcX anti-mouse CD16/32 (Biolegend 101319) and

524   LIVE/DEAD Fixable Aqua (Invitrogen L34957) per the manufacturer's instructions. For each of

525   the respective screens, stimulated library was stained for its respective marker with the following

526   antibody: MHCII (APC anti-mouse I-A/I-E Antibody, Clone M5/114.15.2 Biolegend 107613),

527   CD40 (APC anti-mouse CD40 Antibody, Clone 3/23 Biolegend 124611), or PD-L1 (APC anti-

528   mouse CD274 (B7-H1, PD-L1) Antibody, Clone 10F.9G2 Biolegend 124311). Each antibody

529   was titrated for optimal staining using the isogenic L3 macrophage cell line. Following staining,

530   cells were fixed in 4% paraformaldehyde. High and low expressing populations were isolated by

531   fluorescence activated cell sorting (FACS) using a BD FACS Aria II Cell Sorter. Bin size was

532   guided by control cells which were unstimulated and to ensure sufficient library coverage (>25x

533   unselected library, or >2e6 cells per bin). Following isolation of sorted populations,

534   paraformaldehyde crosslinks were reversed by incubation in proteinase K (Qiagen) at 55 degrees

535   for 6-8 hours. Subsequently, genomic DNA was isolated using DNeasy Blood and Tissue Kit

536   (Qiagen 69504) according to the manufacturer's instructions. Amplification of sgRNAs by PCR

537   was performed as previously described(74, 126) using Illumina compatible primers from IDT,

538   and amplicons were sequenced on an Illumina NextSeq500. Sequence reads were trimmed to

539   remove adapter sequence and to adjust for staggered forward (p5) primer using Cutadapt v2.9.

540   Raw sgRNA counts for each sorted and unsorted (input library) population was quantified using

541   bowtie2 via MAGeCK to map reads to the sgRNA library index (no mismatch allowed); a

542   sgRNAindex was modified to reflect genes transcribed by our macrophage cell line either basally

543   or upon stimulation with IFNγ as previously published(79). Counts for sgRNAs were median

544   normalized to account for variable sequencing depth.

545

546   **MAGeCK-MLE**

547   We used MAGeCK-MLE to test for gene enrichment. Two separate analyses were performed in

548   order to: (1) identify regulators of the IFNγ response, and (2) identify specific regulators of each

549   of the screen targets. For both analyses, the baseline samples were the input libraries from each

550   of the replicate screens in order to account for slight variabilities in library distribution for each

551   screen. For (1), the generalized linear model was based on a design matrix that was "marker-

552   blind" and only considered the bin of origin (i.e. MHCII-low, CD40-low, PD-L1-low v. MHCII-

553   high, CD40-high, PD-L1-high). For (2), the design matrix was "marker-aware and bin-specific"

554   to test for marker-specific differences (i.e. MHCII-low v. CD40-low v. PD-L1-low); the analysis

555   was performed separately for each bin, low or high expressing mutants, to identify marker-

556   specific positive and negative regulators, respectively. For each analysis, β scores (selection co-

557   efficient) for each gene were summed across conditions to allow for simultaneous assessment of

558   positive and negative regulators across conditions. Data are provided in Supplementary Tables.

559

560   Gene-set enrichment analysis (GSEA) was performed using a ranked gene list as calculated from

561   MAGeCK-MLE beta scores and false discovery rate (FDR). To facilitate the identification of

562   positively and negatively enriched gene sets from the high and low expressing populations, the

563   positive ("pos | beta") and negative ("neg | beta") beta scores for each gene were summed as

564   described above ("beta_sum"). To generate a ranked gene list for GSEA, we employed

565   Stouffer's method to sum positive ("pos | z") and negative ("neg | z") selection z-scores, which

566   were used to re-calculate p-values ("p_sum") as has been previously described (127-129). Using

567   these summative metrics, we calculated a gene score as: log10(p_sum) * (beta_sum). Genes were

568   ranked in descending order and GSEA was performed with standard settings including

569   "weighted" enrichment statistic and "meandiv" normalization mode. Analysis was inclusive of

570   gene sets comprising of 10-500 genes that were compiled and made available online by the

571   Bader lab (130, 131).

572

573   **Plasmids and sgRNA cloning**

574   Lentivirus was generated using HEK293T cells using packaging vector psPAX2

575   (Addgene#12260) and envelope plasmid encoding VSV-G. Transfections used TransIT-293

576   (MirusBio MIR 2704) and plasmid ratios according to the manufacturer's instructions. For the

577   generation of retrovirus, pCL-Eco in place of separate packaging and envelope plasmid.

578   Retrovirus encoding the ER-Hoxb8 transgene was kindly provided by David Sykes.

579

580   sgOpti was a gift from Eric Lander & David Sabatini (Addgene plasmid #85681)(132).

581   Individual sgRNAs were cloned as previously described. Briefly, annealed oligos containing the

582   sgRNA targeting sequence were phosphorylated and cloned into a dephosphorylated and BsmBI

583   (New England Biolabs) digested SgOpti (Addgene#85681) which contains a modified sgRNA

584   scaffold for improved sgRNA-Cas9 complexing. Use of sgOpti derivatives for delivery of

585   multiple sgRNAs was performed as detailed elsewhere(79). The sgRNA targeting sequences

586   used for cloning were as follows:

Name/Target	sgRNA sequence
sgIfngr1_1	TATGTGGAGCATAACCGGAG
sgIfngr1_2	GGTATTCCCAGCATACGACA
sgIrf1_1	CTGTAGGTTATACAGATCAG

sgIrf1_2	CGGAGCTGGGCCATTCACAC
sgPtpn2_1	AAGAAGTTACATCTTAACAC
sgPtpn2_2	TGCAGTGATCCATTGCAGTG
sgNdufa1_1	TGTACGCAGTGGACACCCCG
sgNdufa1_2	CGCGTTCCATCAGATACCAC
sgNdufa2_1	GCAGGGATTTCATCGTGCAA
sgNdufa2_2	ATTCGCGGATCAGAATGGGC
sgStat1_1	GGATAGACGCCCAGCCACTG
sgStat1_2	TGTGATGTTAGATAAACAGA
sgOstc_1	GCGTACACCGTCATAGCCGA
sgOstc_2	TCTTACTTCCTCATTACCGG
sgCnbp_1	AGGTAAAACCACCTCTGCCG
sgCnbp_2	GTTGAAGCCTGCTATAACTG

587

588 **Flow cytometry**

589 Cells were harvested at the indicated times post-IFNγ stimulation by scrapping to ensure intact

590 surface proteins. Cells were pelleted and washed with PBS before staining with TruStain FcX

591 anti-mouse CD16/32 (Biolegend 101319) or TruStain FcX anti-human (Biolegend 422301) and

592 LIVE/DEAD Fixable Aqua (Invitrogen L34957) per the manufacturer's instructions. The

593 following antibodies were used as indicated in the figure legends:

594 APC-Fire750 anti-mouse I-A/I-E Antibody, Clone M5/114.15.2 Biolegend 107651

595 PE anti-mouse CD40 Antibody, Clone 3/23 Biolegend 124609

596 Brilliant Violet 421™ anti-mouse CD274 (B7-H1, PD-L1) Antibody, Clone 10F.9G2 Biolegend

597 124315

598 Alexa Fluor® 647 anti-human CD54 Antibody, Clone HCD54, Biolegned 322718

599 PE anti-human CD40 Antibody, Clone 5C3, Biolegned 334307

600 Brilliant Violet 421™ anti-human CD274 (B7-H1, PD-L1) Antibody, Clone 29E.2A3, Biolegend

601 329713

602 APC/Fire™ 750 anti-human HLA-DR Antibody, Clone L243, Biolegend 307657

603

604 For intracellular cytokine staining, cells were treated with brefeldin A (Biolegend 420601) for 5

605 hours before harvesting. Following staining and fixation, cells were permeabilized (Biolegend

606 421002) and stained according to the manufacturer's protocol using the following antibodies:

607 PE anti-mouse IFN-γ Antibody, Biolegend 505807

608

609 Surface protein expression was analyzed on either a MacsQuant Analyzer or Cytek Aurora. All

610 flow cytometry analysis was done in FlowJo V10 (TreeStar).

611

612 **Chemical inhibitors**

613 All chemical inhibitors were used for the duration of cell stimulation unless otherwise stated.

614 Rotenone (Sigma R8875) was resuspended in DMSO and used at 10uM unless indicated

615 otherwise in the figure legend. Oligomycin (Cayman 11342) was resuspended in DMSO and

616 used at 2.5uM unless otherwise indicated. CCCP (Cayman 25458) was resuspended in DMSO

617 and used at 1.5uM unless indicated otherwise. 1400W hydrochloride (Cayman 81520) was

618 resuspended in culture media, filter sterilized and used immediately at 25uM unless otherwise

619 indicated. N-acetyl-L-Cysteine (NAC, Cayman 20261) was resuspended in culture media, filter

620 sterilized and used immediately at 10mM. DMOG (Cayman 71210) was resuspended in DMSO

621 and used at 200uM. UK5099 (Cayman 16980) was resuspended in DMSO and used at 20uM. 2-

622 deoxy-D-Glucose (2DG, Cayman 14325) was resuspended in culture media, filter sterilized and

623 used at 1mM or at the indicated concentrations immediately. MitoTEMPO hydrate (Cayman

624 16621) was resuspended in DMSO and used at the indicated concentrations.

625

626 For experiments that used defined minimal media with carbon supplementation, D-galactose,

627 sodium pyruvate, and D-glucose were used at 10mM in DMEM without any carbon (Gibco

628 A1443001). For establishment of macrophage cell line with diminished mitochondrial mass,

629 cells were continuously cultured in linezolid (LZD) (Kind gift from Clifton Barry) for 4 weeks at

630 50 μg/mL or DMSO control. Both LZD-conditioned and DMSO control lines were

631 supplemented with uridine at 50 μg/mL. Prior to experimentation, cells were washed with PBS

632 and cultured without linezolid for at least 12 hours.

633

634 **ELISA and nitric oxide quantification**

635 The following kits were purchased from R and D Systems or Biolegend for quantifying protein

636 for cell supernatants:

637 Mouse IL-6 DuoSet ELISA (DY406) or Biolegend ELISAmax (431301)

638 Mouse TNF-alpha DuoSet ELISA (DY410) or Biolegend ELISAmax (430901)

639 Mouse IFN-gamma DuoSet ELISA (DY485)

640 Human IL-1 beta/IL-1F2 DuoSet ELISA (DY201)

641 Human TNF-alpha DuoSet ELISA (DY210)

642 Nitric oxide was quantified from cell supernatants using the Griess Reagent System according to

643 the manufacturer's instructions (Promega G2930). For these experiments, cell culture media

644 without phenol red (Gibco A1443001 or Gibco 31053028).

645

646 **RNA isolation and quantitative real-time PCR**

647 To isolate RNA, cells were lysed in TRIzol (15596026) according to manufacturer's instructions.

648 Chloroform was added to lysis at ratio of 200uL chloroform per 1mL TRIzol and centrifuged at

649   12,000 x g for 20 minutes at 4C. The aqueous layer was separated and added to equal volume of

650   100% ethanol. RNA was isolated using the Zymo Research Direct-zol RNA extraction kit.

651   Quantity and purity of the RNA was checked using a NanoDrop and diluted to 5ng/uL in

652   nuclease-free water before use. Quantitative real-time PCR was performed using NEB Luna®

653   Universal One-Step RT-qPCR Kit (E3005) or the Quantitect SYBR green RT-PCR kit (204243)

654   according to the manufacturer's protocol and run on a Viia7 thermocycler or StepOne Plus

655   Theromocycler. Relative gene expression was determined with ddCT method with beta-Actin

656   transcript as the reference.

Primer	Sequence
RT_Actb-1F	GGCTGTATTCCCCTCCATCG
RT_Actb-1R	CCAGTTGGTAACAATGCCATGT
RT_Cd274-1F	GCTCCAAAGGACTTGTACGTG
RT_Cd274-1R	TGATCTGAAGGGCAGCATTTC
RT-Ciita-1F	AGACCTGGATCGTCTCGT
RT-Ciita-1R	AGTGCATGATTTGAGCGTCTC
RT-Gapdh-1F	TGGCCTTCCGTGTTCCTAC
RT-Gapdh-1R	GAGTTGCTGTTGAAGTCGCA

657

658   **Quantification of mitochondrial genomes**

659   Genomic DNA was isolated from cell pellets using the DNeasy Blood and Tissue Kit (Qiagen

660   69504). Quantitative PCR was run using NEB Luna® Universal One-Step RT-qPCR without the

661   RT enzyme mix and run on a Viia7 thermocycler. Relative quantification of mitochondrial

662   genomes was determined by measuring the relative abundance of mitochondrially encoded gene

663   Nd1 to the abundance of nuclear encoded Hk2 as has been described elsewhere(133). All primers

664   are detailed in attached table.

665

Name/Target	Sequence
Mm-Nd1-1F	CTAGCAGAAACAAACCGGGC
Mm-Nd1-1R	CCGGCTGCGTATTCTACGTT
Mm-Hk2-1F	GCCAGCCTCTCCTGATTTTAGTGT
Mm-Hk2-1R	GGGAACACAAAAGACCTCTTCTGG

666

667 **Immunoblot**

668 At the indicated times following stimulation, cells were washed with PBS once and lysed in on

669 ice using the following buffer: 1% Triton X-100, 150mM NaCl, 5mM KCl, 2mM MgCl2, 1mM

670 EDTA, 0.1% SDS, 0.5% DOC, 25mM Tris-HCl, pH 7.4, with protease and phosphatase inhibitor

671 (Sigma #11873580001 and Sigma P5726). Lysates were further homogenized using a 25g needle

672 and cleared by centrifugation before quantification (Pierce™ BCA Protein Assay Kit, 23225).

673 Parallel blots were run with the same samples, 15ug per well. The following antibodies were

674 used according to the manufacturer's instructions:

675 Purified anti-STAT1 Antibody Biolegend Clone A15158C

676 Purified anti-STAT1 Phospho (Ser727) Antibody, Biolegend Clone A15158B

677 Phospho-Stat1 (Tyr701) Rabbit mAb, Cell Signaling Technology Clone 58D6

678 Jak2 XP® Rabbit mAb, Cell Signaling Technology Clone D2E12

679 Phospho-Jak2 (Tyr1007/1008) Antibody, Cell Signaling Technology #3771S

680 Anti-mouse β-Actin Antibody, Santa Cruz Biotechnology Clone C4

681 Biotin anti-mouse CD119 (IFN-γ R α chain) Antibody, Biolegend Clone 2E2

682 Goat anti-Rabbit IgG (H+L) Secondary Antibody, HRP, Invitrogen 31460

683 Goat anti-Mouse IgG (H+L) Secondary Antibody, HRP, Invitrogen 31430

684 HRP-Conjugated Streptavidin, Thermo Scientific N100

685

686   **Bioenergetics Assay**

687   Relative glycolytic and respiratory capacity were determined as has previously been

688   demonstrated(134). Briefly, cellular ATP levels were determined using CellTiter-Glo® 2.0 Cell

689   Viability Assay (Promega G9241) according to the manufacturer's protocol. Cells were grown in

690   the conditions indicated in the figure legends for 4 hours unless stated otherwise. ATP levels

691   were normalized according to the figure legend.

692

693   **T cell activation assay**

694   We used a previously established co-culture system to assess antigen presentation to Ag-specific

695   T cells. Briefly, C7 CD4+ T cells were isolated from transgenic C7 mice, respectively and

696   stimulated in vitro with irradiated splenocytes pulsed with the ESAT-61-15 peptide, in complete

697   media (RPMI with 10% FBS) containing IL-2 and IL-7. After the initial stimulation, the T cells

698   were split every two days for 3-4 divisions and rested for two to three weeks. After the initial

699   stimulation, the cells were cultured in complete media containing IL-2 and IL-7. The following

700   synthetic peptide epitopes were used as antigens from New England Peptide (Gardener, MA):

701   ESAT-61-15 (MTEQQWNFAGIEAAA).

702   For use in co-culture assay, T cells were added to peptide-pulsed macrophages as described in

703   figure legends at an effector to target ratio of 1:1. Following 1 hours of co-culture, brefeldin A

704   was added for 5 hours before assessing intracellular cytokine production by ICS.

705

706   **Quantification of subunit effects on N-module**

707   We used publicly available proteomics data in which the protein abundance of all complex I

708   subunit was measured when each subunit was genetically deleted(93). As determined empirically

709   by the authors, the N-module components included: NDUFA1, NDUFA2, NDUFS1, NDUFV2,

710   NDUFA6, NDUFS6, NDUFA7, NDUFS4, and NDUFV3. The relative effect of each subunit

711   (using a knockout of that subunit) on N-module protein stability was calculated as the sum of the

712   median log2 ratio of each of the above mentioned subunits, minus the median log2 ratio of itself

713   (since it is knocked out).

714

715   **Statistical Analysis and Figures**

716   Statistical analysis was done using Prism Version 8 (GraphPad) as indicated in the figure

717   legends. Data are presented, unless otherwise indicated, as the mean +/- the standard deviation.

718   Figures were created in Prism V8 or R (Version 3.6.2). MAGeCK-MLE was used as part of

719   MAGeCK-FLUTE package v1.8.0.

720

731 **Competing Interests**

732 The authors have no competing interests related to the research described in this manuscript.

733

734   **Figure Legends:**

735   **Figure 1. Forward genetic screen to identify regulators of the IFNγ response**. A)

736   Representative histograms of the three selected cell surface markers targeted in macrophage

737   CRISPR screens: MHCII, CD40, and PD-L1. Blue histograms indicate expression of each

738   marker in unstimulated macrophages and alternatively colored histograms show expression

739   following 24 hour stimulation with recombinant murine IFNγ (10ng/mL). Gates used for sorting

740   "high" and "low" populations are shown. B) Schematic of CRISPR screens. C) Relative

741   enrichment of select positive control (points) and all 1000 non-targeting control sgRNAs (gray

742   distribution) are plotted as a function of their log2 fold enrichment ("high" vs "low" bins). Data

743   are from both replicate selections for each sgRNA (sgRNA denoted by shape). D) Heatmap of β

744   scores from CRISPR analysis, ordered according to k-means clustering (k=8) of the 5% most

745   enriched or depleted genes in each screen. E) Macrophages were stimulated for 24 hours with

746   TNF (25ng/mL), IFNγ (10ng/mL) or both TNF and IFNγ. Mean fluorescence intensity (MFI) of

747   CD40 and MHCII were quantified by flow cytometry. Data are mean ± the standard deviation for

748   3 biological replicates. Representative scatter plot from two independent experiments is

749   provided. F) Macrophages transduced with sgRNA targeting *Stat1, Ostc, Cnbp*, or a NTC control

750   were cultured with or without IFNγ for 24 hours and cell surface expression of PD-L1 (MFI) was

751   quantified by flow cytometry. For each genotype, data are the mean of cell lines with two

752   independent sgRNAs ± the standard deviation. Data are representative of three independent

753   experiments. Statistical testing in panel C was performed with Tukey's multiple comparisons

754   test. Within each screen, the sgRNA effects for each gene were compared to the distribution non-

755   targeting control sgRNAs. Statistical testing in panels E and F was performed by one-way

756   ANOVA with Holm-Sidak multiple comparisons correction. p values of 0.05, 0.01, 0.001, and

757   0.001are indicated by *, **, ***, and ****

758

759   **Figure 2. Global analysis of knockout libraries implicates mitochondrial complex I is a**

760   **positive regulator of the IFNγ response.** A) Rank plot of the combined analysis for all genome-

761   wide knockout screens. Gene ranks (x-axis) were determined by maximal likelihood estimation

762   (MLE). Known positive (left) and negative (right) regulators of IFNγ-mediated signaling are

763   highlighted. The q-value (false discovery rate) for each gene is indicated by dot size (-Log_{10}

764   FDR). B). Gene set enrichment analysis (GSEA) is based on the ranked list of positive

765   regulators. Non-redundant pathways with a normalized enrichment score (NES) exceeding 2.0

766   and a false discovery rate (FDR) below 0.025 are labeled. C) Relative enrichment (log2 fold

767   change between "high" and "low" bins) of genes which comprise the mitochondrial respirasome

768   (GeneOntology 0005746) and were targeted in the CRISPR KO library. Respirasome

769   components are grouped by ETC complex. FDR is based on MAGeCK-MLE. D) Screen-specific

770   enrichment score is plotted for Complex I structural subunits and assembly factors. The

771   statistical enrichment of a gene (e.g. *Ndufa1*) or module (e.g. N) was calculated using a binomial

772   distribution function to calculate the probability that observed sgRNAs under examination would

773   be depleted or enriched given the expected median probability. P values of 0.05, 0.01, 0.001, and

774   0.001are indicated by *, **, ***, and ****. E) Correlation between the relative effect of each

775   complex I subunit on the structural integrity of the N-module (x-axis) with the relative

776   requirement of each complex I subunit for the IFNγ-response (y-axis; β score, as in Panel D).

777   The Pearson correlation coefficient (r) was calculated to be 0.6452 (95% confidence interval

778   0.3584 to 0.8207; p-value = 0.0002. As *Ndufab1* (empty square) is an essential gene, its

779   detection in the library indicates editing did not eliminate function; therefore, it was excluded

780   from correlation analysis.

781

782   **Figure 3. Complex I is necessary for IFNγ-induced MHCII and PD-L1 expression.**

783   Metabolic phenotypes in macrophage mutants were confirmed using ATP abundance following

784   culture in media containing only (A) glucose or (B) pyruvate. Values are normalized to the

785   average respiratory capacity of non-targeting control macrophages (NTC) and are the mean ± the

786   standard deviation for 4 biological replicates. Statistical testing within each condition (with or

787   without IFNγ for 24h) was performed by one-way ANOVA with Dunnett's multiple comparisons

788   correction. (C-F) Non-targeting control (NTC), positive control (sg*Ifngr1* and sg*Ptpn2*) and

789   complex I mutant (sg*Ndufa1* and sg*Ndufa2*) macrophages were stimulated for 24 hours with

790   recombinant murine IFNγ. Plotted values in C and E are the geometric mean fluorescence

791   intensity (MFI) for a given mutant normalized to an internal control present in each well; for

792   each gene, the data are the mean for two independent sgRNAs ± the standard deviation.

793   Representative histograms are provided in D and F. Data are representative of >5 independent

794   experiments. G) MHCII MFI of macrophages stimulated with IFNγ and treated with rotenone at

795   the indicated concentrations for 24 hours. Mean ± the standard deviation for 2 biological

796   replicates are shown. Data are representative of four independent experiments. H) Left: MHCII

797   MFI on macrophages cultured in complete media (CM) and stimulated with IFNγ and the

798   indicated inhibitors for 24 hours. Right: MHCII MFI on macrophages cultured in CM or media

799   containing only pyruvate (Pyr) or citrate (Cit) with or without UK5099 and stimulated with

800   IFNγ for 24 hours. Mean ± standard deviation for 2 or 3 biological replicates is indicated. Data

801   are representative of four independent experiments. Statistical testing was performed by one-way

802   ANOVA with Tukey correction for multiple hypothesis testing. p values of 0.05, 0.01, 0.001,

803   and 0.001are indicated by *, **, ***, and ****.

804

805   **Figure 4. Diminished mitochondrial function specifically limits IFNγ-dependent responses.**

806   A) TNF and IL-6 production by NTC or complex I mutant macrophages stimulated with

807   Pam3CSK4 for 24 hours was determined by ELISA. Statistical testing between mutant and NTC

808   macrophages from triplicate samples was performed by ANOVA with Dunnett's correction for

809   multiple comparisons. Data are representative of two independent experiments. B) qPCR

810   determination of relative mitochondrial genomes present per nuclear genome in macrophages

811   cultured in vehicle (WT) or 50 ug/mL linezolid (LZD). C_t values were normalized to reference

812   nuclear gene hexokinase 2 (*Hk2*) and plotted as abundance relative to WT. Data were analyzed

813   by two-way unpaired t-test. C) ATP abundance in control or LZD-conditioned macrophages

814   cultured in 10mM glucose, galactose or pyruvate. ATP values normalized to mean of 10mM

815   glucose and plotted as percent. Mean ± the standard deviation for 2 biological replicates of each

816   condition. Differences were tested by two-way ANOVA using the Sidak method to correct for

817   multiple hypothesis testing. D) MFI of MHCII was determined by flow cytometry on control or

818   LZD-conditioned macrophages following 24 hour stimulation with IFNγ. Mean ± the standard

819   deviation for 2 biological replicates of each condition and representative of two independent

820   experiments. Differences were tested by two-way ANOVA using the Tukey method to correct

821   for multiple hypothesis testing. E and F) Secretion of TNF and IL-6 in WT and LZD-conditioned

822   macrophages following Pam3CSK4 stimulation for 6 hours was quantified by ELISA. Mean ±

823   the standard deviation for 3 biological replicates of each condition and two independent

824   experiments. Data were analyzed by two-way unpaired t-test. p values of 0.05, 0.01, 0.001, and

825   0.001are indicated by *, **, ***, and ****.

826

827 **Figure 5. Complex I is specifically required for IFNγ signaling in human cells.** A) CD14+

828 monocytes from healthy human donors were differentiated into macrophages. MFI of cell

829 surface markers PD-L1, ICAM1, CD40 and HLA-DR was determined by flow cytometry

830 following stimulation with IFNγ and/or inhibition of complex I with rotenone (10uM) for 24

831 hours. Data are representative of two independent experiments and values are normalized to

832 donor-specific unstimulated/vehicle control. Mean ± the standard deviation for 6 biological

833 replicates of each condition. Differences were tested by two-way ANOVA using the Sidak-Holm

834 method to correct for multiple hypothesis testing. B and C) Quantification of IL-1B and TNF

835 production from primary human macrophages, measured by ELISA from cell supernatants

836 following stimulation. Lines connect values for individual donors treated with vehicle (DMSO,

837 black squares) or rotenone (empty squares). Differences were tested by repeat-measure two-way

838 ANOVA using the Sidak-Holm method to correct for multiple hypothesis testing. p values of

839 0.05, 0.01, 0.001, and 0.001are indicated by *, **, ***, and ****.

840   **Figure 6. Complex I inhibition reduces IFNγ receptor activity.** A) PD-L1 transcript was

841   quantified by qRT-PCR using ΔΔCt relative to *β-Actin* in macrophages of the indicated genotype

842   after stimulation with 10ng/mL IFNγ. PD-L1 MFI was determined at the same time points by

843   flow cytometry. B) *Ciita* transcript was quantified by qRT-PCR using ΔΔCt relative to *β-Actin*

844   *Gapdh* in macrophages of the indicated genotype after stimulation with 10ng/mL IFNγ. MHCII

845   MFI was determined at the same time points by flow cytometry. Data shown are from biological

846   triplicate samples with technical replicates for RT-PCR experiments and are representative of

847   two independent experiments. C) sgNTC (left) or sg*Irf1* (right) macrophages were cultured for

848   24 hours with or without IFNγ stimulation. At 2 hour intervals post-IFNγ stimulation, rotenone

849   was added. After 24 hours of stimulation, cells were harvested and surface expression of MHCII

850   (MFI) was quantified by flow cytometry. Data are mean ± the standard deviation for 3 biological

851   replicates and are representative of two independent experiments. Statistical testing was

852   performed by one-way ANOVA with Tukey correction for multiple hypothesis testing. D)

853   Control (NTC) or sg*Ndufa1* macrophages were stimulated with IFNγ for the indicated times, and

854   cell lysates analyzed by immunoblot for STAT1 abundance and phosphorylation (Y701 and

855   S727), JAK2 abundance and phosphorylation (Y1007/8), and IFNGR1. Beta-Actin was used as a

856   loading control. Data are representative of three independent experiments. Results shown are

857   from a single experiment analyzed on three parallel blots. p values of 0.05, 0.01, 0.001, and

858   0.001are indicated by *, **, ***, and ****.

859

860   **Figure 7. Mitochondrial respiration in antigen presenting cells is required IFNγ-dependent**

861   **T cell activation.** A) Cell surface expression of MHCII (MFI) in macrophages (MF) or dendritic

862   cells (DC) derived from conditionally immortalized progenitor lines. IFNγ was added for 24

863   hours where indicated. Cells were treated with vehicle (DMSO), rotenone (10uM), oligomycin

864   (OM, 2.5uM), or CCCP concurrent with IFNγ. Data are three biological replicates and are

865   representative of at least two independent experiments. B) Contour plot of macrophage (top row)

866   or dendritic cell (bottom row) MHCII expression in the absence of (left column) or following

867   (right column) stimulation with IFNγ for 24 hours. Representative samples were selected from

868   (A). The percent MHCII positive are indicated for each of the conditions. C) CD4+ T cell

869   activation as measured by the percent of live cells positive for IFNγ by intracellular cytokine

870   staining. Prior to co-culture with T cells, APCs were stimulated with the indicated combinations

871   of IFNγ (10ng/mL), and/or rotenone (10uM) for 24 hours. After washing and pulsing with

872   ESAT-61-15 at the indicated concentrations (nm.), T cells were added to APCs at an effector to

873   target (E:T) ratio of 1:1, and co-cultured for a total of 5 hours. Data are representative of two

874   independent experiments. Data are mean ± the standard deviation for 3 biological replicates.

875   Statistical testing was performed by one-way ANOVA with Tukey correction for multiple

876   hypothesis testing. D and E) sg*Ndufa1* or NTC macrophages were differentiated from

877   immortalized progenitors, and mixed at the ratios indicated (labeled as percent of KO cells).

878   Mixed cultures were stimulated with IFNγ for 24 hours, peptide loaded, and co-cultured with

879   CD4+ T cells (E:T 1:1). Production of IFNγ was measured by ICS and quantified as the percent

880   of cells positive for staining by flow cytometry. Representative contour plots (D) and

881   quantification (E) of the experiment are shown. Data shown are for biological triplicate samples

882   and are representative of two independent experiments. p values of 0.05, 0.01, 0.001, and

883   0.001are indicated by *, **, ***, and ****.

884

885

886   **Supplementary Figure Legends:**

887   **Figure S1, Related to Figure 3. A)** sgNTC, sg*Ndufa1*, sg*Ndufa2* cells cultured in complete

888   media and treated with or without oligomycin (2.5μM) for 4 hours. Relative ATP levels were

889   determined as in Figure 2A **B)** Intracellular ATP levels quantified as relative light units (RLU)

890   using CellTiterGlo2.0 (Promega) for macrophages in specified growth conditions for 4 hours.

891   Concentrations of carbon source and inhibitors are indicated in Materials and Methods. **C)**

892   Macrophages were cultured in either glucose or galactose and stimulated with IFNγ for 24 hours.

893   Following stimulation, the proportion of cells with MHCII expression was determined by flow

894   cytometry. **D)** Macrophages were cultured in conditions as described in Figure 4H. For each

895   condition, cells were stimulated with IFNγ or IFNγ and N-acetylcysteine (NAC) for 24 hours

896   after which cell surface levels of MHCII were quantified. **E)** Control or complex I mutant

897   (sg*Ndufa2*) macrophages were stimulated with IFNγ for 24 hours with increasing doses of

898   mitochondrial reactive oxygen species scavenger MitoTempo. For each concentration, values are

899   plotted as a fold change relative to no scavenger; Mean ± the standard deviation for 2 biological

900   replicates of each condition. **F)** Control or complex I deficient macrophages were stimulated

901   with IFNγ for 24 hours with or without the addition of DMOG or 1400W. Following stimulation,

902   the proportion of cells with MHCII expression was determined by flow cytometry. G) Nitric

903   oxide was measured using Griess Reagent System (Promega) from cell supernatants following

904   stimulation with IFNγ and Pam3CSK4 for 24 hours with or without the addition of DMOG or

905   1400W. Relative nitric oxide levels were calculated as a percent relative to control (IFNγ and

906   Pam3CSK4 with DMSO). All data are representative of at least two independent experiments.

907   Statistical testing was performed using one-way ANOVA with Holm-Sidak multiple comparison

908   correction. p values of 0.05, 0.01, 0.001, and 0.001are indicated by *, **, ***, and ****.

909

910

911   **Figure S2, Related to Figure 7.** A-C) Myeloid progenitors cells were conditionally

912   immortalized by transducing murine bone marrow with an estrogen-dependent Hoxb8 transgene

913   which maintains stem-like properties. Following differentiation of progenitors into macrophages

914   using M-CSF enriched conditioned media, macrophages were stimulated with IFNγ with or

915   without rotenone. 24 hours after stimulation, cell surface levels of (A) MHCII, (B) CD40, (C)

916   and PD-L1 were quantified by flow cytometry. Data are representative of 3 independent

917   experiments and are the mean ± the standard deviation for 2 biological replicates. Statistical

918   testing was performed by one-way ANOVA with Tukey correction for multiple hypothesis

919   testing. D-F) As in panels A-C, macrophages from either immortalized macrophage progenitors

920   or primary bone marrow were stimulated with IFNγ with or without rotenone or oligomycin. 24

921   hours after stimulation, cell surface levels of (D) MHCII, (E) CD40, (F) and PD-L1 were

922   quantified by flow cytometry. G). Wild-type or ΔNdufa1 macrophages derived from Hoxb8-

923   immortalized bone marrow progenitors were cultured in the specified media and inhibitor

924   condition before total intracellular ATP was quantified by CellTiterGlo2.0. For each genotype,

925   values are relative to "glucose" control. Mean ± the standard deviation for 2 biological replicates

926   of each condition. p values of 0.05, 0.01, 0.001, and 0.001are indicated by *, **, ***, and ****.

927

928

929
930

931

Bibliography

1. Mechanisms of costimulation, (2009).
2. Attanasio J, Wherry EJ. Costimulatory and Coinhibitory Receptor Pathways in Infectious Disease. Immunity. 2016;44(5):1052-68. Epub 2016/05/19. doi: 10.1016/j.immuni.2016.04.022. PubMed PMID: 27192569; PMCID: PMC4873956.
3. Genetic control of MHC class II expression, (2002).
4. Buxadé M, Encabo HH, Riera-Borrull M, Quintana-Gallardo L, López-Cotarelo P, Tellechea M, Martínez-Martínez S, Redondo JM, Martín-Caballero J, Flores JM, Bosch E, Rodríguez-Fernández JL, Aramburu J, López-Rodríguez C. Macrophage-specific MHCII expression is regulated by a remote Ciita enhancer controlled by NFAT5. Journal of Experimental Medicine. 2018. doi: 10.1084/jem.20180314. PubMed PMID: 30327417.
5. Herrero C, Marqués L, Lloberas J, Celada A. IFN-γ-dependent transcription of MHC class II IA is impaired in macrophages from aged mice. Journal of Clinical Investigation. 2001. doi: 10.1172/JCI11696. PubMed PMID: 11181648.
6. Regulation of MHC class II gene expression by the class II transactivator, (2005).
7. Present Yourself! By MHC Class I and MHC Class II Molecules, (2016).
8. Steimle V, Siegrist CA, Mottet A, Lisowska-Grospierre B, Mach B. Regulation of MHC class II expression by interferon-γ mediated by the transactivator gene CIITA. Science. 1994. doi: 10.1126/science.8016643. PubMed PMID: 8016643.
9. Wheelock EF. Interferon-Like Virus-Inhibitor Induced in Human Leukocytes by Phytohemagglutinin. Science. 1965;149(3681):310-1. Epub 1965/07/16. doi: 10.1126/science.149.3681.310. PubMed PMID: 17838106.
10. Tominaga K, Yoshimoto T, Torigoe K, Kurimoto M, Matsui K, Hada T, Okamura H, Nakanishi K. IL-12 synergizes with IL-18 or IL-1beta for IFN-gamma production from human T cells. Int Immunol. 2000;12(2):151-60. Epub 2000/02/02. doi: 10.1093/intimm/12.2.151. PubMed PMID: 10653850.
11. O'Shea JJ, Paul WE. Regulation of T(H)1 differentiation--controlling the controllers. Nat Immunol. 2002;3(6):506-8. Epub 2002/05/29. doi: 10.1038/ni0602-506. PubMed PMID: 12032561.
12. Schneider BE, Korbel D, Hagens K, Koch M, Raupach B, Enders J, Kaufmann SHE, Mittrücker HW, Schaible UE. A role for IL-18 in protective immunity against Mycobacterium tuberculosis. European Journal of Immunology. 2010. doi: 10.1002/eji.200939583.
13. Interleukin-12 and the regulation of innate resistance and adaptive immunity, (2003).
14. Johnson-Léger C, Hasbold J, Holman M, Klaus GG. The effects of IFN-gamma on CD40-mediated activation of B cells from X-linked immunodeficient or normal mice. The Journal of Immunology. 1997;159:1150-9.
15. Alderson MR, Armitage RJ, Tough TW, Strockbine L, Fanslow WC, Spriggs MK. CD40 expression by human monocytes: regulation by cytokines and activation of monocytes by the ligand for CD40. Journal of Experimental Medicine. 1993;178(2):669-74. doi: 10.1084/jem.178.2.669.
16. Yamazaki T, Akiba H, Iwai H, Matsuda H, Aoki M, Tanno Y, Shin T, Tsuchiya H, Pardoll DM, Okumura K, Azuma M, Yagita H. Expression of programmed death 1 ligands by

976 murine T cells and APC. J Immunol. 2002;169(10):5538-45. Epub 2002/11/08. doi:
977 10.4049/jimmunol.169.10.5538. PubMed PMID: 12421930.

978 17. Cross-regulation of Signaling Pathways by Interferon-γ: Implications for Immune
979 Responses and Autoimmune Diseases, (2009).

980 18. Krawczyk CM, Holowka T, Sun J, Blagih J, Amiel E, DeBerardinis RJ, Cross JR, Jung E,
981 Thompson CB, Jones RG, Pearce EJ. Toll-like receptor-induced changes in glycolytic
982 metabolism regulate dendritic cell activation. Blood. 2010. doi: 10.1182/blood-2009-10-
983 249540. PubMed PMID: 20351312.

984 19. Liu P-S, Wang H, Li X, Chao T, Teav T, Christen S, Di Conza G, Cheng W-C, Chou C-H,
985 Vavakova M, Muret C, Debackere K, Mazzone M, Huang H-D, Fendt S-M, Ivanisevic J,
986 Ho P-C. a-ketoglutarate orchestrates macrophage activation through metabolic and
987 epigenetic reprogramming. nature immunology. 2017;18. doi: 10.1038/ni.3796.

988 20. The role of B7 co-stimulation in activation and differentiation of CD4+ and CD8+ T cells,
989 (1998).

990 21. Nau GJ, Richmond JFL, Schlesinger A, Jennings EG, Lander ES, Young RA. Human
991 macrophage activation programs induced by bacterial pathogens. Proceedings of the
992 National Academy of Sciences of the United States of America. 2002;99:1503-8. doi:
993 10.1073/pnas.022649799. PubMed PMID: 11805289.

994 22. Schnare M, Barton GM, Holt AC, Takeda K, Akira S, Medzhitov R. Toll-like receptors
995 control activation of adaptive immune responses. Nature Immunology. 2001. doi:
996 10.1038/ni712. PubMed PMID: 11547333.

997 23. Francisco LM, Sage PT, Sharpe AH. The PD-1 pathway in tolerance and autoimmunity.
998 Immunol Rev. 2010;236:219-42. Epub 2010/07/20. doi: 10.1111/j.1600-
999 065X.2010.00923.x. PubMed PMID: 20636820; PMCID: PMC2919275.

1000 24. Dendritic cells giveth and taketh away, (2005).

1001 25. Brown JA, Dorfman DM, Ma F-R, Sullivan EL, Munoz O, Wood CR, Greenfield EA,
1002 Freeman GJ. Blockade of Programmed Death-1 Ligands on Dendritic Cells Enhances T
1003 Cell Activation and Cytokine Production. The Journal of Immunology. 2003;170:1257-66.
1004 doi: 10.4049/jimmunol.170.3.1257.

1005 26. Schildberg FA, Klein SR, Freeman GJ, Sharpe AH. Coinhibitory Pathways in the B7-CD28
1006 Ligand-Receptor Family. Immunity. 2016;44(5):955-72. Epub 2016/05/19. doi:
1007 10.1016/j.immuni.2016.05.002. PubMed PMID: 27192563; PMCID: PMC4905708.

1008 27. Bousoik E, Montazeri Aliabadi H. "Do We Know Jack" About JAK? A Closer Look at
1009 JAK/STAT Signaling Pathway. Frontiers in Oncology. 2018. doi:
1010 10.3389/fonc.2018.00287.

1011 28. Garcia-Diaz A, Shin DS, Moreno BH, Saco J, Escuin-Ordinas H, Rodriguez GA, Zaretsky
1012 JM, Sun L, Hugo W, Wang X, Parisi G, Saus CP, Torrejon DY, Graeber TG, Comin-
1013 Anduix B, Hu-Lieskovan S, Damoiseaux R, Lo RS, Ribas A. Interferon Receptor Signaling
1014 Pathways Regulating PD-L1 and PD-L2 Expression. Cell Reports. 2017. doi:
1015 10.1016/j.celrep.2017.04.031. PubMed PMID: 28494868.

1016 29. Ealick SE, Cook WJ, Vijay-Kumar S, Carson M, Nagabhushan TL, Trotta PP, Bugg CE.
1017 Three-dimensional structure of recombinant human interferon-gamma. Science.
1018 1991;252(5006):698-702. Epub 1991/05/03. doi: 10.1126/science.1902591. PubMed
1019 PMID: 1902591.

30. Pestka S, Krause CD, Walter MR. Interferons, interferon-like cytokines, and their receptors. Immunol Rev. 2004;202:8-32. Epub 2004/11/18. doi: 10.1111/j.0105-2896.2004.00204.x. PubMed PMID: 15546383.

31. Blouin CM, Lamaze C. Interferon gamma receptor: the beginning of the journey. Front Immunol. 2013;4:267. Epub 2013/09/13. doi: 10.3389/fimmu.2013.00267. PubMed PMID: 24027571; PMCID: PMC3760442.

32. Lasfar A, Cook JR, Cohen Solal KA, Reuhl K, Kotenko SV, Langer JA, Laskin DL. Critical role of the endogenous interferon ligand-receptors in type I and type II interferons response. Immunology. 2014;142(3):442-52. Epub 2014/03/07. doi: 10.1111/imm.12273. PubMed PMID: 24597649; PMCID: PMC4080960.

33. Meraz MA, White JM, Sheehan KC, Bach EA, Rodig SJ, Dighe AS, Kaplan DH, Riley JK, Greenlund AC, Campbell D, Carver-Moore K, DuBois RN, Clark R, Aguet M, Schreiber RD. Targeted disruption of the Stat1 gene in mice reveals unexpected physiologic specificity in the JAK-STAT signaling pathway. Cell. 1996;84(3):431-42. Epub 1996/02/09. doi: 10.1016/s0092-8674(00)81288-x. PubMed PMID: 8608597.

34. Schroder K, Hertzog PJ, Ravasi T, Hume DA. Interferon-gamma: an overview of signals, mechanisms and functions. J Leukoc Biol. 2004;75(2):163-89. Epub 2003/10/04. doi: 10.1189/jlb.0603252. PubMed PMID: 14525967.

35. Lehtonen A, Matikainen S, Julkunen I. Interferons up-regulate STAT1, STAT2, and IRF family transcription factor gene expression in human peripheral blood mononuclear cells and macrophages. Journal of immunology (Baltimore, Md : 1950). 1997. PubMed PMID: 9218597.

36. Chen J, Feng Y, Lu L, Wang H, Dai L, Li Y, Zhang P. Interferon-γ-induced PD-L1 surface expression on human oral squamous carcinoma via PKD2 signal pathway. Immunobiology. 2012;217(4):385-93. Epub 2011/12/30. doi: 10.1016/j.imbio.2011.10.016. PubMed PMID: 22204817.

37. Walser TC, Ma X, Kundu N, Dorsey R, Goloubeva O, Fulton AM. Immune-mediated modulation of breast cancer growth and metastasis by the chemokine Mig (CXCL9) in a murine model. J Immunother. 2007;30(5):490-8. Epub 2007/06/26. doi: 10.1097/CJI.0b013e318031b551. PubMed PMID: 17589289.

38. Lyford-Pike S, Peng S, Young GD, Taube JM, Westra WH, Akpeng B, Bruno TC, Richmon JD, Wang H, Bishop JA, Chen L, Drake CG, Topalian SL, Pardoll DM, Pai SI. Evidence for a role of the PD-1:PD-L1 pathway in immune resistance of HPV-associated head and neck squamous cell carcinoma. Cancer Res. 2013;73(6):1733-41. Epub 2013/01/05. doi: 10.1158/0008-5472.Can-12-2384. PubMed PMID: 23288508; PMCID: PMC3602406.

39. Garrido F, Ruiz-Cabello F, Cabrera T, Pérez-Villar JJ, López-Botet M, Duggan-Keen M, Stern PL. Implications for immunosurveillance of altered HLA class I phenotypes in human tumours. Immunol Today. 1997;18(2):89-95. Epub 1997/02/01. doi: 10.1016/s0167-5699(96)10075-x. PubMed PMID: 9057360.

40. Beatty GL, Paterson Y. Regulation of tumor growth by IFN-gamma in cancer immunotherapy. Immunol Res. 2001;24(2):201-10. Epub 2001/10/12. doi: 10.1385/ir:24:2:201. PubMed PMID: 11594457.

41. Pollard KM, Cauvi DM, Toomey CB, Morris KV, Kono DH. Interferon-γ and systemic autoimmunity. Discov Med. 2013;16(87):123-31. Epub 2013/09/04. PubMed PMID: 23998448; PMCID: PMC3934799.

42. Lees JR, Cross AH. A little stress is good: IFN-gamma, demyelination, and multiple sclerosis. J Clin Invest. 2007;117(2):297-9. Epub 2007/02/03. doi: 10.1172/jci31254. PubMed PMID: 17273549; PMCID: PMC1783822.

43. Bustamante J, Boisson-Dupuis S, Abel L, Casanova J-L. Mendelian susceptibility to mycobacterial disease: genetic, immunological, and clinical features of inborn errors of IFN-γ immunity. Seminars in Immunology. 2014;26(6):454 - 70.

44. Newport MJ, Huxley CM, Huston S, Hawrylowicz CM, Oostra BA, Williamson R, Levin M. A Mutation in the Interferon-γ –Receptor Gene and Susceptibility to Mycobacterial Infection. New England Journal of Medicine. 1996;335(26):1941-9. doi: 10.1056/nejm199612263352602. PubMed PMID: 8960473.

45. Jouanguy E, Altare F, Lamhamedi S, Revy P, Emile J-F, Newport M, Levin M, Blanche S, Seboun E, Fischer A, Casanova J-L. Interferon-γ –Receptor Deficiency in an Infant with Fatal Bacille Calmette–Guérin Infection. New England Journal of Medicine. 1996;335(26):1956-62. doi: 10.1056/nejm199612263352604. PubMed PMID: 8960475.

46. Alcaïs A, Fieschi C, Abel L, Casanova J-L. Tuberculosis in children and adults: two distinct genetic diseases. The Journal of experimental medicine. 2005;202:1617-21. doi: 10.1084/jem.20052302. PubMed PMID: 16365144.

47. Bogunovic D, Byun M, Durfee LA, Abhyankar A, Sanal O, Mansouri D, Salem S, Radovanovic I, Grant AV, Adimi P, Mansouri N, Okada S, Bryant VL, Kong X-F, Kreins A, Velez MM, Boisson B, Khalilzadeh S, Ozcelik U, Darazam IA, Schoggins JW, Rice CM, Al-Muhsen S, Behr M, Vogt G, Puel A, Bustamante J, Gros P, Huibregtse JM, Abel L, Boisson-Dupuis S, Casanova J-L. Mycobacterial Disease and Impaired IFN-γ Immunity in Humans with Inherited ISG15 Deficiency. Science. 2012;337.

48. Filipe-Santos O, Bustamante J, Chapgier A, Vogt G, de Beaucoudrey L, Feinberg J, Jouanguy E, Boisson-Dupuis S, Fieschi C, Picard C, Casanova J-L. Inborn errors of IL-12/23- and IFN-gamma-mediated immunity: molecular, cellular, and clinical features. Seminars in immunology. 2006;18:347-61. doi: 10.1016/j.smim.2006.07.010. PubMed PMID: 16997570.

49. Kong XF, Vogt G, Itan Y, Macura-Biegun A, Szaflarska A, Kowalczyk D, Chapgier A, Abhyankar A, Furthner D, Djambas Khayat C, Okada S, Bryant VL, Bogunovic D, Kreins A, Moncada-Vélez M, Migaud M, Al-Ajaji S, Al-Muhsen S, Holland SM, Abel L, Picard C, Chaussabel D, Bustamante J, Casanova JL, Boisson-Dupuis S. Haploinsufficiency at the human IFNGR2 locus contributes to mycobacterial disease. Human Molecular Genetics. 2013. doi: 10.1093/hmg/dds484.

50. Sharpe AH. Introduction to checkpoint inhibitors and cancer immunotherapy. Immunol Rev. 2017;276(1):5-8. Epub 2017/03/05. doi: 10.1111/imr.12531. PubMed PMID: 28258698; PMCID: PMC5362112.

51. Castro F, Cardoso AP, Goncalves RM, Serre K, Oliveira MJ. Interferon-Gamma at the Crossroads of Tumor Immune Surveillance or Evasion. Front Immunol. 2018;9:847. Epub 2018/05/22. doi: 10.3389/fimmu.2018.00847. PubMed PMID: 29780381; PMCID: PMC5945880.

52. George S, Miao D, Demetri GD, Adeegbe D, Rodig SJ, Shukla S, Lipschitz M, Amin-Mansour A, Raut CP, Carter SL, Hammerman P, Freeman GJ, Wu CJ, Ott PA, Wong KK, Van Allen EM. Loss of PTEN Is Associated with Resistance to Anti-PD-1 Checkpoint Blockade Therapy in Metastatic Uterine Leiomyosarcoma. Immunity. 2017;46:197-204. doi: 10.1016/j.immuni.2017.02.001. PubMed PMID: 28228279.

53. Gong B, Kiyotani K, Sakata S, Nagano S, Kumehara S, Baba S, Besse B, Yanagitani N, Friboulet L, Nishio M, Takeuchi K, Kawamoto H, Fujita N, Katayama R. Secreted PD-L1 variants mediate resistance to PD-L1 blockade therapy in non-small cell lung cancer. Journal of Experimental Medicine. 2019. doi: 10.1084/jem.20180870.

54. IFNγ: signalling, epigenetics and roles in immunity, metabolism, disease and cancer immunotherapy, (2018).

55. Mahoney KM, Shukla SA, Patsoukis N, Chaudhri A, Browne EP, Arazi A, Eisenhaure TM, Pendergraft WF, Hua P, Pham HC, Bu X, Zhu B, Hacohen N, Fritsch EF, Boussiotis VA, Wu CJ, Freeman GJ. A secreted PD-L1 splice variant that covalently dimerizes and mediates immunosuppression. Cancer Immunology, Immunotherapy. 2019. doi: 10.1007/s00262-018-2282-1. PubMed PMID: 30564891.

56. Guak H, Al Habyan S, Ma EH, Aldossary H, Al-Masri M, Won SY, Ying T, Fixman ED, Jones RG, McCaffrey LM, Krawczyk CM. Glycolytic metabolism is essential for CCR7 oligomerization and dendritic cell migration. Nat Commun. 2018;9(1):2463. Epub 2018/06/27. doi: 10.1038/s41467-018-04804-6. PubMed PMID: 29941886; PMCID: PMC6018630.

57. Balic JJ, Albargy H, Luu K, Kirby FJ, Jayasekara WSN, Mansell F, Garama DJ, Nardo DD, Baschuk N, Louis C, Humphries F, Fitzgerald K, Latz E, Gough DJ, Mansell A. metabolic reprogramming and IL-1 β expression. Nature Communications. 2020;11:1-11. doi: 10.1038/s41467-020-17669-5.

58. Carneiro FRG, Lepelley A, Seeley JJ, Hayden MS, Ghosh S. An Essential Role for ECSIT in Mitochondrial Complex I Assembly and Mitophagy in Macrophages. Cell Rep. 2018;22(10):2654-66. Epub 2018/03/08. doi: 10.1016/j.celrep.2018.02.051. PubMed PMID: 29514094; PMCID: PMC5909989.

59. Everts B, Amiel E, Huang SCC, Smith AM, Chang CH, Lam WY, Redmann V, Freitas TC, Blagih J, Van Der Windt GJW, Artyomov MN, Jones RG, Pearce EL, Pearce EJ. TLR-driven early glycolytic reprogramming via the kinases TBK1-IKKε supports the anabolic demands of dendritic cell activation. Nature Immunology. 2014;15:323-32. doi: 10.1038/ni.2833. PubMed PMID: 24562310.

60. Everts B, Amiel E, van der Windt GJ, Freitas TC, Chott R, Yarasheski KE, Pearce EL, Pearce EJ. Commitment to glycolysis sustains survival of NO-producing inflammatory dendritic cells. Blood. 2012;120(7):1422-31. Epub 2012/07/13. doi: 10.1182/blood-2012-03-419747. PubMed PMID: 22786879; PMCID: PMC3423780.

61. Jha AK, Huang SC, Sergushichev A, Lampropoulou V, Ivanova Y, Loginicheva E, Chmielewski K, Stewart KM, Ashall J, Everts B, Pearce EJ, Driggers EM, Artyomov MN. Network integration of parallel metabolic and transcriptional data reveals metabolic modules that regulate macrophage polarization. Immunity. 2015;42(3):419-30. Epub 2015/03/19. doi: 10.1016/j.immuni.2015.02.005. PubMed PMID: 25786174.

62. Liu PS, Wang H, Li X, Chao T, Teav T, Christen S, Di Conza G, Cheng WC, Chou CH, Vavakova M, Muret C, Debackere K, Mazzone M, Huang HD, Fendt SM, Ivanisevic J, Ho PC. alpha-ketoglutarate orchestrates macrophage activation through metabolic and epigenetic reprogramming. Nat Immunol. 2017;18(9):985-94. Epub 2017/07/18. doi: 10.1038/ni.3796. PubMed PMID: 28714978.

63. Mills EL, Kelly B, Logan A, Costa ASH, Varma M, Bryant CE, Tourlomousis P, Dabritz JHM, Gottlieb E, Latorre I, Corr SC, McManus G, Ryan D, Jacobs HT, Szibor M, Xavier RJ, Braun T, Frezza C, Murphy MP, O'Neill LA. Succinate Dehydrogenase Supports

1158   Metabolic Repurposing of Mitochondria to Drive Inflammatory Macrophages. Cell.
1159   2016;167(2):457-70 e13. Epub 2016/09/27. doi: 10.1016/j.cell.2016.08.064. PubMed
1160   PMID: 27667687; PMCID: PMC5863951.
1161 64. Jung SB, Choi MJ, Ryu D, Yi HS, Lee SE, Chang JY, Chung HK, Kim YK, Kang SG, Lee
1162   JH, Kim KS, Kim HJ, Kim CS, Lee CH, Williams RW, Kim H, Lee HK, Auwerx J, Shong
1163   M. Reduced oxidative capacity in macrophages results in systemic insulin resistance. Nat
1164   Commun. 2018;9(1):1551. Epub 2018/04/21. doi: 10.1038/s41467-018-03998-z. PubMed
1165   PMID: 29674655; PMCID: PMC5908799.
1166 65. Palmieri EM, Gonzalez-Cotto M, Baseler WA, Davies LC, Ghesquiere B, Maio N, Rice
1167   CM, Rouault TA, Cassel T, Higashi RM, Lane AN, Fan TW, Wink DA, McVicar DW.
1168   Nitric oxide orchestrates metabolic rewiring in M1 macrophages by targeting aconitase 2
1169   and pyruvate dehydrogenase. Nat Commun. 2020;11(1):698. Epub 2020/02/06. doi:
1170   10.1038/s41467-020-14433-7. PubMed PMID: 32019928; PMCID: PMC7000728.
1171 66. Wang F, Zhang S, Jeon R, Vuckovic I, Jiang X, Lerman A, Folmes CD, Dzeja PD,
1172   Herrmann J. Interferon Gamma Induces Reversible Metabolic Reprogramming of M1
1173   Macrophages to Sustain Cell Viability and Pro-Inflammatory Activity. EBioMedicine.
1174   2018. doi: 10.1016/j.ebiom.2018.02.009.
1175 67. Baardman J, Verberk SGS, Prange KHM, van Weeghel M, van der Velden S, Ryan DG,
1176   Wust RCI, Neele AE, Speijer D, Denis SW, Witte ME, Houtkooper RH, O'Neill L A,
1177   Knatko EV, Dinkova-Kostova AT, Lutgens E, de Winther MPJ, Van den Bossche J. A
1178   Defective Pentose Phosphate Pathway Reduces Inflammatory Macrophage Responses
1179   during Hypercholesterolemia. Cell Rep. 2018;25(8):2044-52 e5. Epub 2018/11/22. doi:
1180   10.1016/j.celrep.2018.10.092. PubMed PMID: 30463003.
1181 68. Cheng SC, Quintin J, Cramer RA, Shepardson KM, Saeed S, Kumar V, Giamarellos-
1182   Bourboulis EJ, Martens JHA, Rao NA, Aghajanirefah A, Manjeri GR, Li Y, Ifrim DC, Arts
1183   RJW, Van Der Meer BMJW, Deen PMT, Logie C, O'Neill LA, Willems P, Van De
1184   Veerdonk FL, Van Der Meer JWM, Ng A, Joosten LAB, Wijmenga C, Stunnenberg HG,
1185   Xavier RJ, Netea MG. MTOR- and HIF-1α-mediated aerobic glycolysis as metabolic basis
1186   for trained immunity. Science. 2014. doi: 10.1126/science.1250684. PubMed PMID:
1187   25258083.
1188 69. Mills EL, Ryan DG, Prag HA, Dikovskaya D, Menon D, Zaslona Z, Jedrychowski MP,
1189   Costa ASH, Higgins M, Hams E, Szpyt J, Runtsch MC, King MS, McGouran JF, Fischer
1190   R, Kessler BM, McGettrick AF, Hughes MM, Carroll RG, Booty LM, Knatko EV, Meakin
1191   PJ, Ashford MLJ, Modis LK, Brunori G, Sévin DC, Fallon PG, Caldwell ST, Kunji ERS,
1192   Chouchani ET, Frezza C, Dinkova-Kostova AT, Hartley RC, Murphy MP, O'Neill LA.
1193   Itaconate is an anti-inflammatory metabolite that activates Nrf2 via alkylation of KEAP1.
1194   Nature. 2018. doi: 10.1038/nature25986. PubMed PMID: 29590092.
1195 70. Tannahill GM, Curtis AM, Adamik J, Palsson-Mcdermott EM, McGettrick AF, Goel G,
1196   Frezza C, Bernard NJ, Kelly B, Foley NH, Zheng L, Gardet A, Tong Z, Jany SS, Corr SC,
1197   Haneklaus M, Caffrey BE, Pierce K, Walmsley S, Beasley FC, Cummins E, Nizet V,
1198   Whyte M, Taylor CT, Lin H, Masters SL, Gottlieb E, Kelly VP, Clish C, Auron PE, Xavier
1199   RJ, O'Neill LAJ. Succinate is an inflammatory signal that induces IL-1β through HIF-1α.
1200   Nature. 2013. doi: 10.1038/nature11986. PubMed PMID: 23535595.
1201 71. Veldhoen M, Blankenhaus B, Konjar S, Ferreira C. Metabolic wiring of murine T cell and
1202   intraepithelial lymphocyte maintenance and activation. Eur J Immunol. 2018;48(9):1430-
1203   40. Epub 2018/07/26. doi: 10.1002/eji.201646745. PubMed PMID: 30043974.

1204 72. Buck MD, O'Sullivan D, Pearce EL. T cell metabolism drives immunity. J Exp Med.
1205   2015;212(9):1345-60. Epub 2015/08/12. doi: 10.1084/jem.20151159. PubMed PMID:
1206   26261266; PMCID: PMC4548052.
1207 73. Su X, Yu Y, Zhong Y, Giannopoulou EG, Hu X, Liu H, Cross JR, Rätsch G, Rice CM,
1208   Ivashkiv LB. Interferon-γ regulates cellular metabolism and mRNA translation to
1209   potentiate macrophage activation. Nat Immunol. 2015;16(8):838-49. Epub 2015/07/07. doi:
1210   10.1038/ni.3205. PubMed PMID: 26147685; PMCID: PMC4509841.
1211 74. Doench JG, Fusi N, Sullender M, Hegde M, Vaimberg EW, Donovan KF, Smith I, Tothova
1212   Z, Wilen C, Orchard R, Virgin HW, Listgarten J, Root DE. Optimized sgRNA design to
1213   maximize activity and minimize off-target effects of CRISPR-Cas9. Nat Biotechnol.
1214   2016;34(2):184-91. Epub 2016/01/19. doi: 10.1038/nbt.3437. PubMed PMID: 26780180;
1215   PMCID: PMC4744125.
1216 75. Li W, Koster J, Xu H, Chen CH, Xiao T, Liu JS, Brown M, Liu XS. Quality control,
1217   modeling, and visualization of CRISPR screens with MAGeCK-VISPR. Genome Biol.
1218   2015;16:281. Epub 2015/12/18. doi: 10.1186/s13059-015-0843-6. PubMed PMID:
1219   26673418; PMCID: PMC4699372.
1220 76. Ferwerda G, Girardin SE, Kullberg BJ, Le Bourhis L, De Jong DJ, Langenberg DML, Van
1221   Crevel R, Adema GJ, Ottenhoff THM, Van Der Meer JWM, Netea MG. NOD2 and toll-
1222   like receptors are nonredundant recognition systems of Mycobacterium tuberculosis. PLoS
1223   Pathogens. 2005. doi: 10.1371/journal.ppat.0010034.
1224 77. Chapoval AI, Ni J, Lau JS, Wilcox RA, Flies DB, Liu D, Dong H, Sica GL, Zhu G,
1225   Tamada K, Chen L. B7-H3: A costimulatory molecule for T cell activation and IFN-γ
1226   production. Nature Immunology. 2001. doi: 10.1038/85339. PubMed PMID: 11224528.
1227 78. Steimle V, Durand B, Barras E, Zufferey M, Hadam MR, Mach B, Reith W. A novel DNA-
1228   binding regulatory factor is mutated in primary MHC class II deficiency (bare lymphocyte
1229   syndrome). Genes and Development. 1995. doi: 10.1101/gad.9.9.1021. PubMed PMID:
1230   7744245.
1231 79. Kiritsy MC, Ankley LM, Trombley JD, Huizinga GP, Lord AE, Orning P, Elling R,
1232   Fitzgerald KA, Olive AJ. A genome-wide screen in macrophages identifies new regulators
1233   of IFNγ-inducible MHCII that contribute to T cell activation. bioRxiv. 2020.
1234 80. Gu W, Chen J, Yang L, Zhao KN. TNF-alpha promotes IFN-gamma-induced CD40
1235   expression and antigen process in Myb-transformed hematological cells.
1236   ScientificWorldJournal. 2012;2012:621969. Epub 2012/05/02. doi: 10.1100/2012/621969.
1237   PubMed PMID: 22547990; PMCID: PMC3322478.
1238 81. Kataoka K, Shiraishi Y, Takeda Y, Sakata S, Matsumoto M, Nagano S, Maeda T, Nagata
1239   Y, Kitanaka A, Mizuno S, Tanaka H, Chiba K, Ito S, Watatani Y, Kakiuchi N, Suzuki H,
1240   Yoshizato T, Yoshida K, Sanada M, Itonaga H, Imaizumi Y, Totoki Y, Munakata W,
1241   Nakamura H, Hama N, Shide K, Kubuki Y, Hidaka T, Kameda T, Masuda K, Minato N,
1242   Kashiwase K, Izutsu K, Takaori-Kondo A, Miyazaki Y, Takahashi S, Shibata T,
1243   Kawamoto H, Akatsuka Y, Shimoda K, Takeuchi K, Seya T, Miyano S, Ogawa S. Aberrant
1244   PD-L1 expression through 3′-UTR disruption in multiple cancers. Nature. 2016;534:402-6.
1245   doi: 10.1038/nature18294. PubMed PMID: 27281199.
1246 82. Burr ML, Sparbier CE, Chan YC, Williamson JC, Woods K, Beavis PA, Lam EYN,
1247   Henderson MA, Bell CC, Stolzenburg S, Gilan O, Bloor S, Noori T, Morgens DW, Bassik
1248   MC, Neeson PJ, Behren A, Darcy PK, Dawson SJ, Voskoboinik I, Trapani JA, Cebon J,

1249   Lehner PJ, Dawson MA. CMTM6 maintains the expression of PD-L1 and regulates anti-
1250   Tumour immunity. Nature. 2017. doi: 10.1038/nature23643. PubMed PMID: 28813417.
1251 83. Coelho MA, de Carné Trécesson S, Rana S, Zecchin D, Moore C, Molina-Arcas M, East P,
1252   Spencer-Dene B, Nye E, Barnouin K, Snijders AP, Lai WS, Blackshear PJ, Downward J.
1253   Oncogenic RAS Signaling Promotes Tumor Immunoresistance by Stabilizing PD-L1
1254   mRNA. Immunity. 2017;47:1083-99.e6. doi: 10.1016/j.immuni.2017.11.016.
1255 84. Manguso RT, Pope HW, Zimmer MD, Brown FD, Yates KB, Miller BC, Collins NB, Bi K,
1256   LaFleur MW, Juneja VR, Weiss SA, Lo J, Fisher DE, Miao D, Van Allen E, Root DE,
1257   Sharpe AH, Doench JG, Haining WN. In vivo CRISPR screening identifies Ptpn2 as a
1258   cancer immunotherapy target. Nature. 2017;547(7664):413-8. Epub 2017/07/21. doi:
1259   10.1038/nature23270. PubMed PMID: 28723893; PMCID: PMC5924693.
1260 85. Mezzadra R, Sun C, Jae LT, Gomez-Eerland R, De Vries E, Wu W, Logtenberg MEW,
1261   Slagter M, Rozeman EA, Hofland I, Broeks A, Horlings HM, Wessels LFA, Blank CU,
1262   Xiao Y, Heck AJR, Borst J, Brummelkamp TR, Schumacher TNM. Identification of
1263   CMTM6 and CMTM4 as PD-L1 protein regulators. Nature. 2017. doi:
1264   10.1038/nature23669. PubMed PMID: 28813410.
1265 86. Hassounah NB, Malladi VS, Huang Y, Freeman SS, Beauchamp EM, Koyama S, Souders
1266   N, Martin S, Dranoff G, Wong KK, Pedamallu CS, Hammerman PS, Akbay EA.
1267   Identification and characterization of an alternative cancer-derived PD-L1 splice variant.
1268   Cancer Immunology, Immunotherapy. 2019. doi: 10.1007/s00262-018-2284-z. PubMed
1269   PMID: 30564890.
1270 87. Kriegsman BA, Vangala P, Chen BJ, Meraner P, Brass AL, Garber M, Rock KL. Frequent
1271   Loss of IRF2 in Cancers Leads to Immune Evasion through Decreased MHC Class I
1272   Antigen Presentation and Increased PD-L1 Expression. The Journal of Immunology.
1273   2019;203:1999-2010. doi: 10.4049/jimmunol.1900475. PubMed PMID: 31471524.
1274 88. Papalexi E, Mimitou E, Butler AW, Foster S, Bracken B, Mauck WM, Wessels H-H,
1275   Yeung BZ, Smibert P, Satija R. Characterizing the molecular regulation of inhibitory
1276   immune checkpoints with multi-modal single-cell screens. bioRxiv.
1277   2020:2020.06.28.175596. doi: 10.1101/2020.06.28.175596.
1278 89. Wang P, Geng J, Gao J, Zhao H, Li J, Shi Y, Yang B, Xiao C, Linghu Y, Sun X, Chen X,
1279   Hong L, Qin F, Li X, Yu JS, You H, Yuan Z, Zhou D, Johnson RL, Chen L. Macrophage
1280   achieves self-protection against oxidative stress-induced ageing through the Mst-Nrf2 axis.
1281   Nat Commun. 2019;10(1):755. Epub 2019/02/16. doi: 10.1038/s41467-019-08680-6.
1282   PubMed PMID: 30765703; PMCID: PMC6376064.
1283 90. Wijdeven RH, van Luijn MM, Wierenga-Wolf AF, Akkermans JJ, van den Elsen PJ,
1284   Hintzen RQ, Neefjes J. Chemical and genetic control of IFNgamma-induced MHCII
1285   expression. EMBO Rep. 2018;19(9). Epub 2018/07/20. doi: 10.15252/embr.201745553.
1286   PubMed PMID: 30021835; PMCID: PMC6123650.
1287 91. Liu B, Liao J, Rao X, Kushner SA, Chung CD, Chang DD, Shuai K. Inhibition of Stat1-
1288   mediated gene activation by PIAS1. Proc Natl Acad Sci U S A. 1998;95(18):10626-31.
1289   Epub 1998/09/02. doi: 10.1073/pnas.95.18.10626. PubMed PMID: 9724754; PMCID:
1290   PMC27945.
1291 92. Subramanian A, Tamayo P, Mootha VK, Mukherjee S, Ebert BL, Gillette MA, Paulovich
1292   A, Pomeroy SL, Golub TR, Lander ES, Mesirov JP. Gene set enrichment analysis: A
1293   knowledge-based approach for interpreting genome-wide expression profiles. Proceedings

1294   of the National Academy of Sciences of the United States of America. 2005. doi:
1295   10.1073/pnas.0506580102. PubMed PMID: 16199517.

1296   93.   Stroud DA, Surgenor EE, Formosa LE, Reljic B, Frazier AE, Dibley MG, Osellame LD,
1297   Stait T, Beilharz TH, Thorburn DR, Salim A, Ryan MT. Accessory subunits are integral for
1298   assembly and function of human mitochondrial complex I. Nature. 2016;538(7623):123-6.
1299   Epub 2016/09/15. doi: 10.1038/nature19754. PubMed PMID: 27626371.

1300   94.   Lazarou M, McKenzie M, Ohtake A, Thorburn DR, Ryan MT. Analysis of the Assembly
1301   Profiles for Mitochondrial- and Nuclear-DNA-Encoded Subunits into Complex I.
1302   Molecular and Cellular Biology. 2007;27:4228-37.

1303   95.   Pagliarini DJ, Calvo SE, Chang B, Sheth SA, Vafai SB, Ong SE, Walford GA, Sugiana C,
1304   Boneh A, Chen WK, Hill DE, Vidal M, Evans JG, Thorburn DR, Carr SA, Mootha VK. A
1305   mitochondrial protein compendium elucidates complex I disease biology. Cell.
1306   2008;134(1):112-23. Epub 2008/07/11. doi: 10.1016/j.cell.2008.06.016. PubMed PMID:
1307   18614015; PMCID: PMC2778844.

1308   96.   Baradaran R, Berrisford JM, Minhas GS, Sazanov LA. Crystal structure of the entire
1309   respiratory complex I. Nature. 2013;494(7438):443-8. doi: 10.1038/nature11871.

1310   97.   Zickermann V, Wirth C, Nasiri H, Siegmund K, Schwalbe H, Hunte C, Brandt U.
1311   Mechanistic insight from the crystal structure of mitochondrial complex I. Science.
1312   2015;347:44-9.

1313   98.   Zhu J, Vinothkumar KR, Hirst J. Structure of mammalian respiratory complex I. Nature.
1314   2016;536(7616):354-8. doi: 10.1038/nature19095.

1315   99.   Barrientos A, Moraes CT. Titrating the effects of mitochondrial complex I impairment in
1316   the cell physiology. J Biol Chem. 1999;274(23):16188-97. Epub 1999/05/29. doi:
1317   10.1074/jbc.274.23.16188. PubMed PMID: 10347173.

1318   100.   Brand MD, Nicholls DG. Assessing mitochondrial dysfunction in cells. Biochem J.
1319   2011;435(2):297-312. Epub 2011/07/06. doi: 10.1042/BJ20110162. PubMed PMID:
1320   21726199; PMCID: PMC3076726.

1321   101.   Vacanti Nathaniel M, Divakaruni Ajit S, Green Courtney R, Parker Seth J, Henry Robert R,
1322   Ciaraldi Theodore P, Murphy Anne N, Metallo Christian M. Regulation of Substrate
1323   Utilization by the Mitochondrial Pyruvate Carrier. Molecular Cell. 2014;56(3):425-35. doi:
1324   https://doi.org/10.1016/j.molcel.2014.09.024.

1325   102.   De Vriese AS, Van Coster R, Smet J, Seneca S, Lovering A, Van Haute LL,
1326   Vanopdenbosch LJ, Martin JJ, Ceuterick-De Groote C, Vandecasteele S, Boelaert JR.
1327   Linezolid-induced inhibition of mitochondrial protein synthesis. Clinical Infectious
1328   Diseases. 2006;42:1111-7. doi: 10.1086/501356.

1329   103.   Soriano A, Miró O, Mensa J. Mitochondrial Toxicity Associated with Linezolid. New
1330   England Journal of Medicine. 2005;353:2305-6. doi: 10.1056/NEJM200511243532123.

1331   104.   Wilson DN, Schluenzen F, Harms JM, Starosta AL, Connell SR, Fucini P. The
1332   oxazolidinone antibiotics perturb the ribosomal peptidyl-transferase center and effect tRNA
1333   positioning. Proc Natl Acad Sci U S A. 2008;105(36):13339-44. Epub 2008/09/02. doi:
1334   10.1073/pnas.0804276105. PubMed PMID: 18757750; PMCID: PMC2533191.

1335   105.   Bustamante E, Morris HP, Pedersen PL. Hexokinase: The Direct Link between
1336   Mitochondrial and Glycolytic Reactions in Rapidly Growing Cancer Cells. Springer,
1337   Boston, MA; 1978. p. 363-80.

1338   106.   Cramer T, Yamanishi Y, Clausen BE, Förster I, Pawlinski R, Mackman N, Haase VH,
1339   Jaenisch R, Corr M, Nizet V, Firestein GS, Gerber HP, Ferrara N, Johnson RS. HIF-1α is

1340   essential for myeloid cell-mediated inflammation. Cell. 2003;112:645-57. doi:
1341   10.1016/S0092-8674(03)00154-5. PubMed PMID: 12628185.

1342   107. Hypoxia-inducible factors in physiology and medicine, (2012).

1343   108. Braverman J, Stanley SA. Nitric Oxide Modulates Macrophage Responses to
1344   Mycobacterium tuberculosis Infection through Activation of HIF-1α and Repression of NF-
1345   κB The Journal of Immunology. 2017. doi: 10.4049/jimmunol.1700515.

1346   109. Mishra BB, Rathinam VAK, Martens GW, Martinot AJ, Kornfeld H, Fitzgerald KA,
1347   Sassetti CM. Nitric oxide controls the immunopathology of tuberculosis by inhibiting
1348   NLRP3 inflammasome-dependent processing of IL-1β. Nature Immunology. 2013. doi:
1349   10.1038/ni.2474.

1350   110. Wang GG, Calvo KR, Pasillas MP, Sykes DB, Häcker H, Kamps MP. Quantitative
1351   production of macrophages or neutrophils ex vivo using conditional Hoxb8. Nature
1352   Methods. 2006. doi: 10.1038/nmeth865.

1353   111. Redecke V, Wu R, Zhou J, Finkelstein D, Chaturvedi V, High AA, Häcker H.
1354   Hematopoietic progenitor cell lines with myeloid and lymphoid potential. Nature Methods.
1355   2013. doi: 10.1038/nmeth.2510.

1356   112. Gallegos AM, Pamer EG, Glickman MS. Delayed protection by ESAT-6-specific effector
1357   CD4+ T cells after airborne M. tuberculosis infection. Journal of Experimental Medicine.
1358   2008. doi: 10.1084/jem.20080353. PubMed PMID: 18779346.

1359   113. Bhat MY, Solanki HS, Advani J, Khan AA, Keshava Prasad TS, Gowda H, Thiyagarajan S,
1360   Chatterjee A. Comprehensive network map of interferon gamma signaling. J Cell Commun
1361   Signal. 2018;12(4):745-51. Epub 2018/09/08. doi: 10.1007/s12079-018-0486-y. PubMed
1362   PMID: 30191398; PMCID: PMC6235777.

1363   114. Cameron AM, Castoldi A, Sanin DE, Flachsmann LJ, Field CS, Puleston DJ, Kyle RL,
1364   Patterson AE, Hässler F, Buescher JM, Kelly B, Pearce EL, Pearce EJ. Inflammatory
1365   macrophage dependence on NAD + salvage is a consequence of reactive oxygen species–
1366   mediated DNA damage. Nature Immunology. 2019. doi: 10.1038/s41590-019-0336-y.

1367   115. Venter G, Oerlemans FTJJ, Willemse M, Wijers M, Fransen JAM, Wieringa B. NAMPT-
1368   Mediated Salvage Synthesis of NAD+ Controls Morphofunctional Changes of
1369   Macrophages. PLoS ONE. 2014;9:e97378. doi: 10.1371/journal.pone.0097378.

1370   116. Minhas PS, Liu L, Moon PK, Joshi AU, Dove C, Mhatre S, Contrepois K, Wang Q, Lee
1371   BA, Coronado M, Bernstein D, Snyder MP, Migaud M, Majeti R, Mochly-Rosen D,
1372   Rabinowitz JD, Andreasson KI. Macrophage de novo NAD(+) synthesis specifies immune
1373   function in aging and inflammation. Nat Immunol. 2019;20(1):50-63. Epub 2018/11/28.
1374   doi: 10.1038/s41590-018-0255-3. PubMed PMID: 30478397; PMCID: PMC6768398.

1375   117. Lv H, Lv G, Chen C, Zong Q, Jiang G, Ye D, Cui X, He Y, Xiang W, Han Q, Tang L,
1376   Yang W, Wang H. NAD(+) Metabolism Maintains Inducible PD-L1 Expression to Drive
1377   Tumor Immune Evasion. Cell Metab. 2020. Epub 2020/11/11. doi:
1378   10.1016/j.cmet.2020.10.021. PubMed PMID: 33171124.

1379   118. Heng TS, Painter MW. The Immunological Genome Project: networks of gene expression
1380   in immune cells. Nat Immunol. 2008;9(10):1091-4. Epub 2008/09/19. doi: 10.1038/ni1008-
1381   1091. PubMed PMID: 18800157.

1382   119. Lipid and small-molecule display by CD1 and MR1, (2015).

1383   120. Benson SA, Ernst JD. TLR2-dependent inhibition of macrophage responses to IFN-γ is
1384   mediated by distinct, gene-specific mechanisms. PLoS ONE. 2009. doi:
1385   10.1371/journal.pone.0006329. PubMed PMID: 19629181.

121. Fortune SM, Solache A, Jaeger A, Hill PJ, Belisle JT, Bloom BR, Rubin EJ, Ernst JD. Mycobacterium tuberculosis Inhibits Macrophage Responses to IFN-γ through Myeloid Differentiation Factor 88-Dependent and -Independent Mechanisms The Journal of Immunology. 2004. doi: 10.4049/jimmunol.172.10.6272. PubMed PMID: 15128816.

122. Kincaid EZ, Wolf AJ, Desvignes L, Mahapatra S, Crick DC, Brennan PJ, Pavelka MS, Jr., Ernst JD. Codominance of TLR2-dependent and TLR2-independent modulation of MHC class II in Mycobacterium tuberculosis infection in vivo. J Immunol. 2007;179(5):3187-95. Epub 2007/08/22. doi: 10.4049/jimmunol.179.5.3187. PubMed PMID: 17709534.

123. Su YM, Teemu P.; Mu, Luye; Mirek, Emily; Manalis, Scott R.; Anthony, Tracy G.; Sesaki, Hiromi; Chen, Jianzhu. Disassembly of ETC Complexes Drives Macrophage Inflammatory Responses by Reprogramming Cellular Metabolism and Translation. Available at SSRN: https://ssrncom/abstract=3611881 or http://dxdoiorg/102139/ssrn3611881. 2020.

124. Jang S, Javadov S. OPA1 regulates respiratory supercomplexes assembly: The role of mitochondrial swelling. Mitochondrion. 2020. doi: 10.1016/j.mito.2019.11.006. PubMed PMID: 31870826.

125. Blasi E, Radzioch D, Merletti L, Varesio L. Generation of macrophage cell line from fresh bone marrow cells with a myc/raf recombinant retrovirus. Cancer biochemistry biophysics. 1989. PubMed PMID: 2695237.

126. Joung J, Konermann S, Gootenberg JS, Abudayyeh OO, Platt RJ, Brigham MD, Sanjana NE, Zhang F. Genome-scale CRISPR-Cas9 knockout and transcriptional activation screening. Nature Protocols. 2017. doi: 10.1038/nprot.2017.016. PubMed PMID: 28333914.

127. Brown MB. 400: A Method for Combining Non-Independent, One-Sided Tests of Significance. Biometrics. 1975;31(4):987-92. doi: 10.2307/2529826.

128. Jia G, Wang X, Xiao G. A permutation-based non-parametric analysis of CRISPR screen data. BMC Genomics. 2017;18(1):545. Epub 2017/07/21. doi: 10.1186/s12864-017-3938-5. PubMed PMID: 28724352; PMCID: PMC5518132.

129. Bodapati S, Daley TP, Lin X, Zou J, Qi LS. A benchmark of algorithms for the analysis of pooled CRISPR screens. Genome Biology. 2020;21(1):62. doi: 10.1186/s13059-020-01972-x.

130. Merico D, Isserlin R, Stueker O, Emili A, Bader GD. Enrichment map: A network-based method for gene-set enrichment visualization and interpretation. PLoS ONE. 2010. doi: 10.1371/journal.pone.0013984. PubMed PMID: 21085593.

131. Reimand J, Isserlin R, Voisin V, Kucera M, Tannus-Lopes C, Rostamianfar A, Wadi L, Meyer M, Wong J, Xu C, Merico D, Bader GD. Pathway enrichment analysis and visualization of omics data using g:Profiler, GSEA, Cytoscape and EnrichmentMap. Nature Protocols. 2019. doi: 10.1038/s41596-018-0103-9. PubMed PMID: 30664679.

132. Fulco CP, Munschauer M, Anyoha R, Munson G, Grossman SR, Perez EM, Kane M, Cleary B, Lander ES, Engreitz JM. Systematic mapping of functional enhancer-promoter connections with CRISPR interference. Science. 2016. doi: 10.1126/science.aag2445.

133. Field CS, Baixauli F, Kyle RL, Puleston DJ, Cameron AM, Sanin DE, Hippen KL, Loschi M, Thangavelu G, Corrado M, Edwards-Hicks J, Grzes KM, Pearce EJ, Blazar BR, Pearce EL. Mitochondrial Integrity Regulated by Lipid Metabolism Is a Cell-Intrinsic Checkpoint for Treg Suppressive Function. Cell Metabolism. 2020. doi: 10.1016/j.cmet.2019.11.021. PubMed PMID: 31883840.

1431   134. Horlbeck MA, Xu A, Wang M, Bennett NK, Park CY, Bogdanoff D, Adamson B, Chow
1432   ED, Kampmann M, Peterson TR, Nakamura K, Fischbach MA, Weissman JS, Gilbert LA.
1433   Mapping the Genetic Landscape of Human Cells. Cell. 2018. doi:
1434   10.1016/j.cell.2018.06.010. PubMed PMID: 30033366.
1435

Figure 1
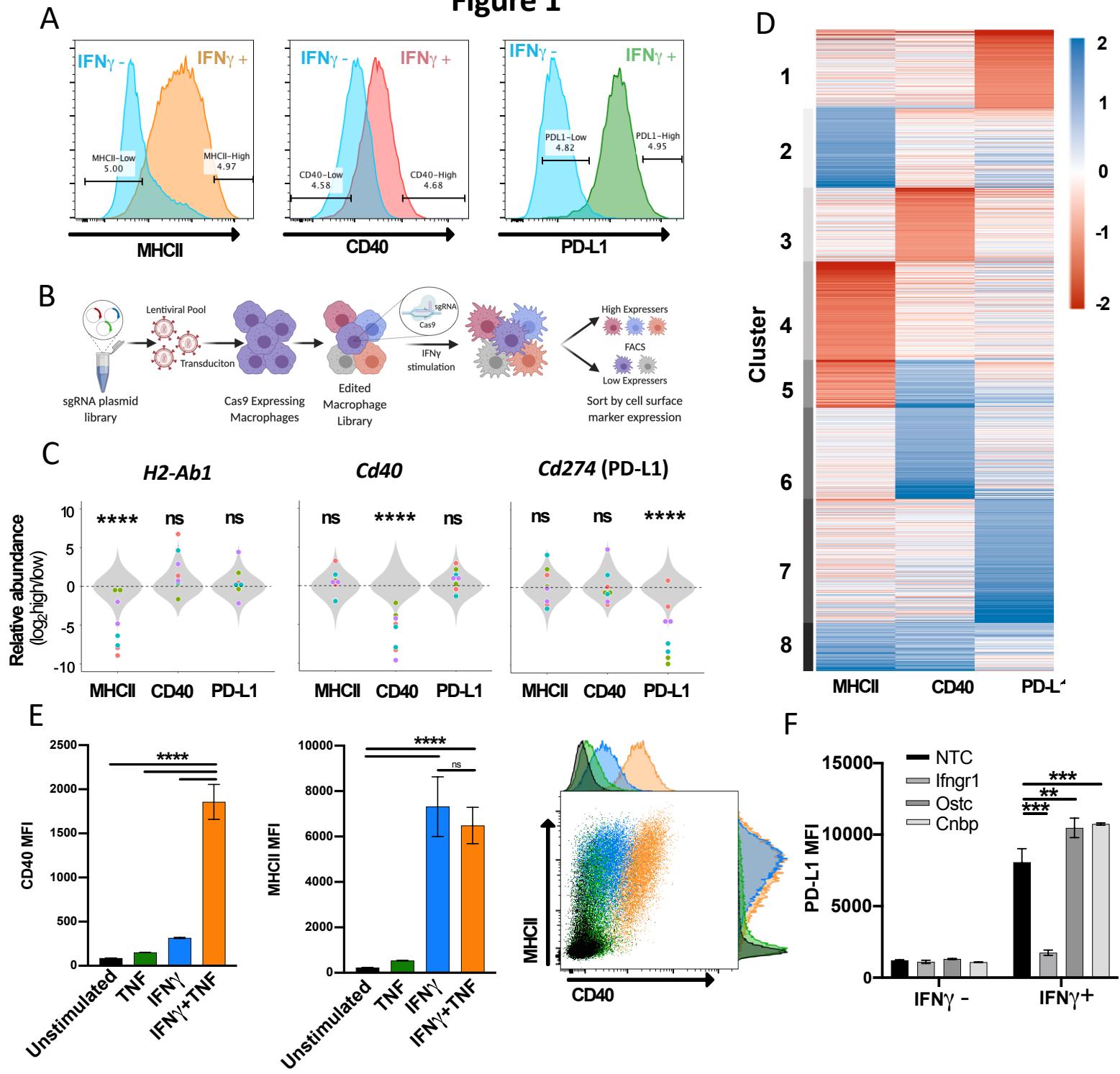
Figure 2
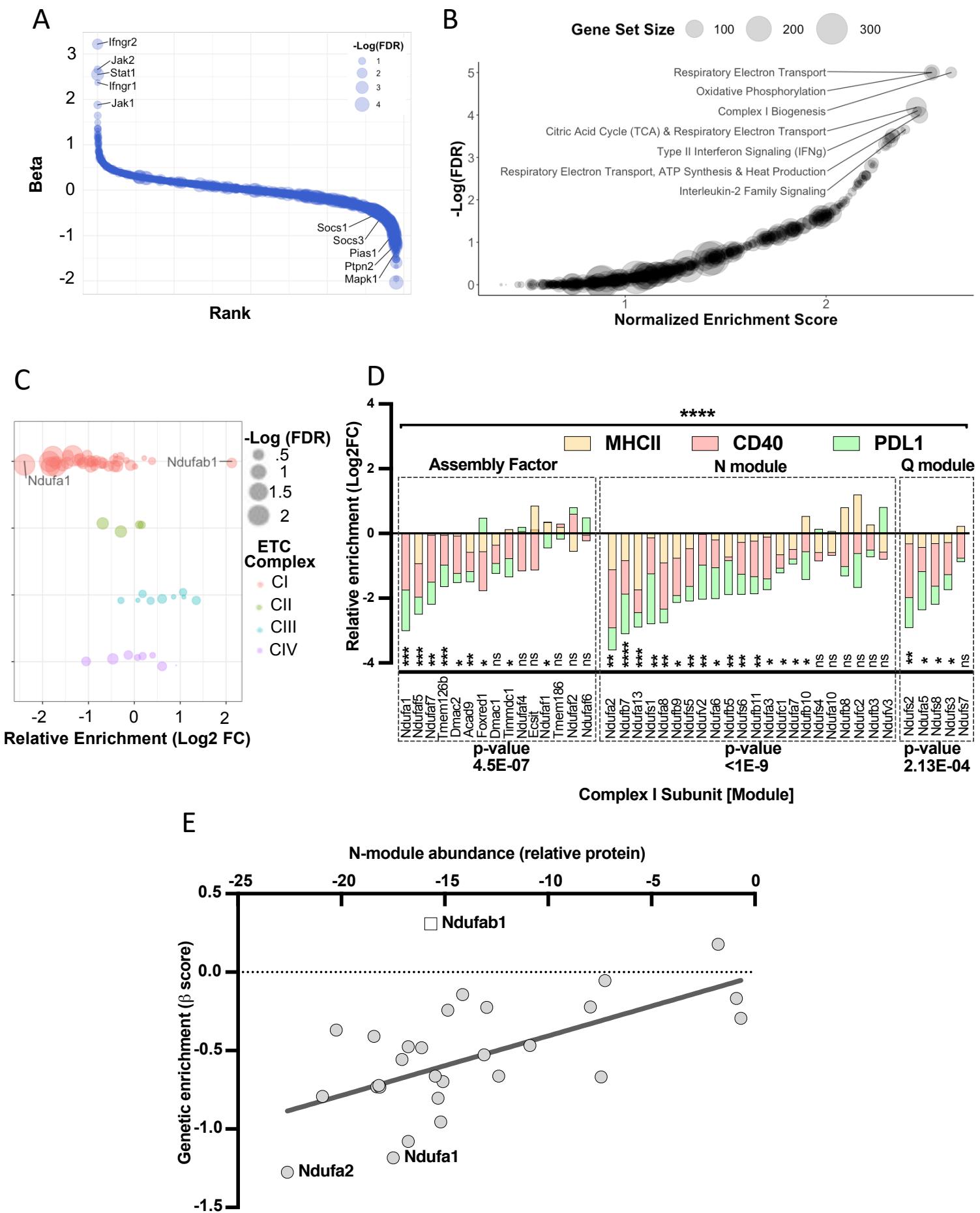
Figure 3
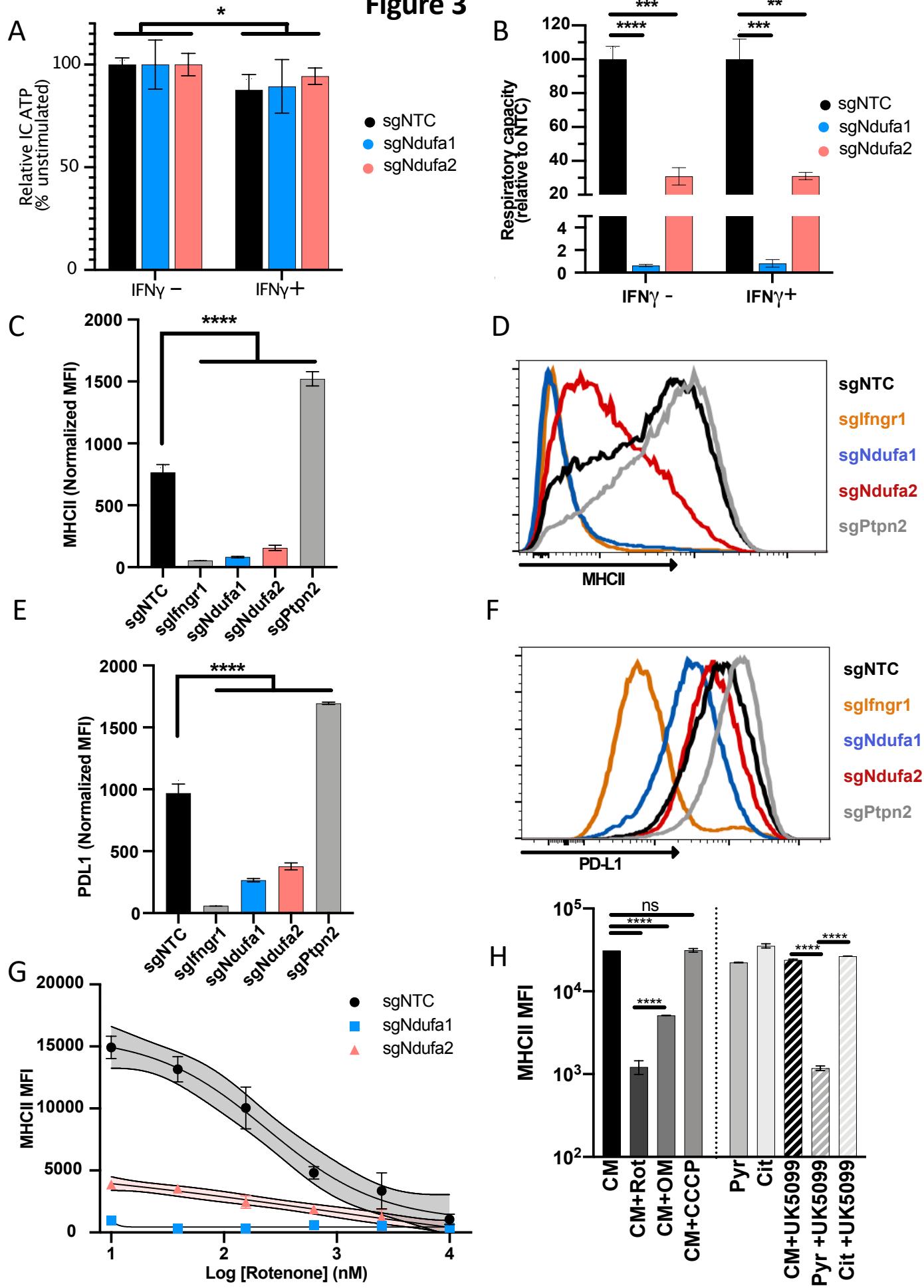
Figure 4
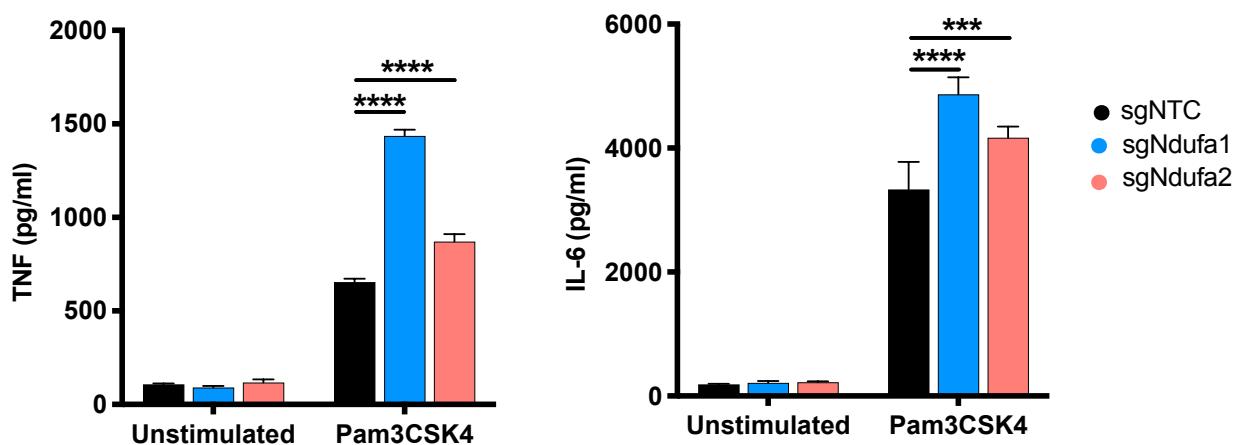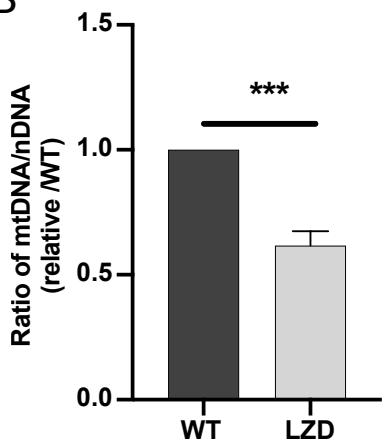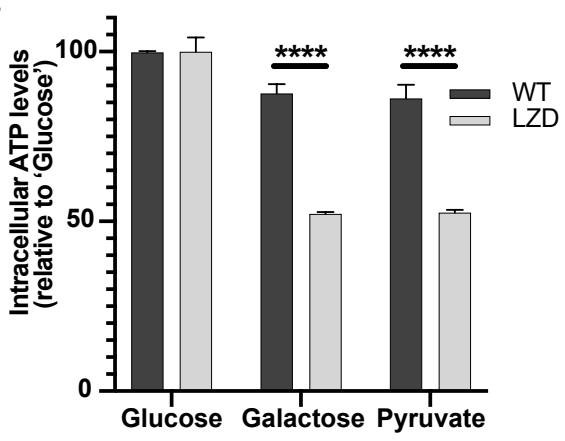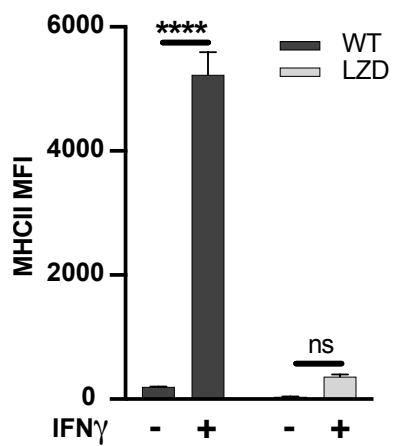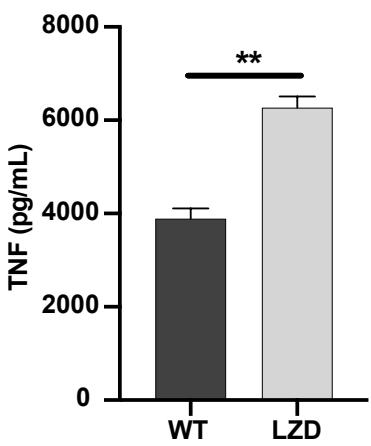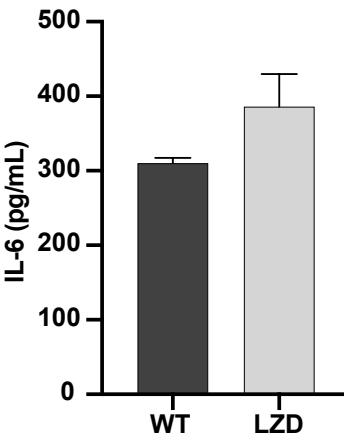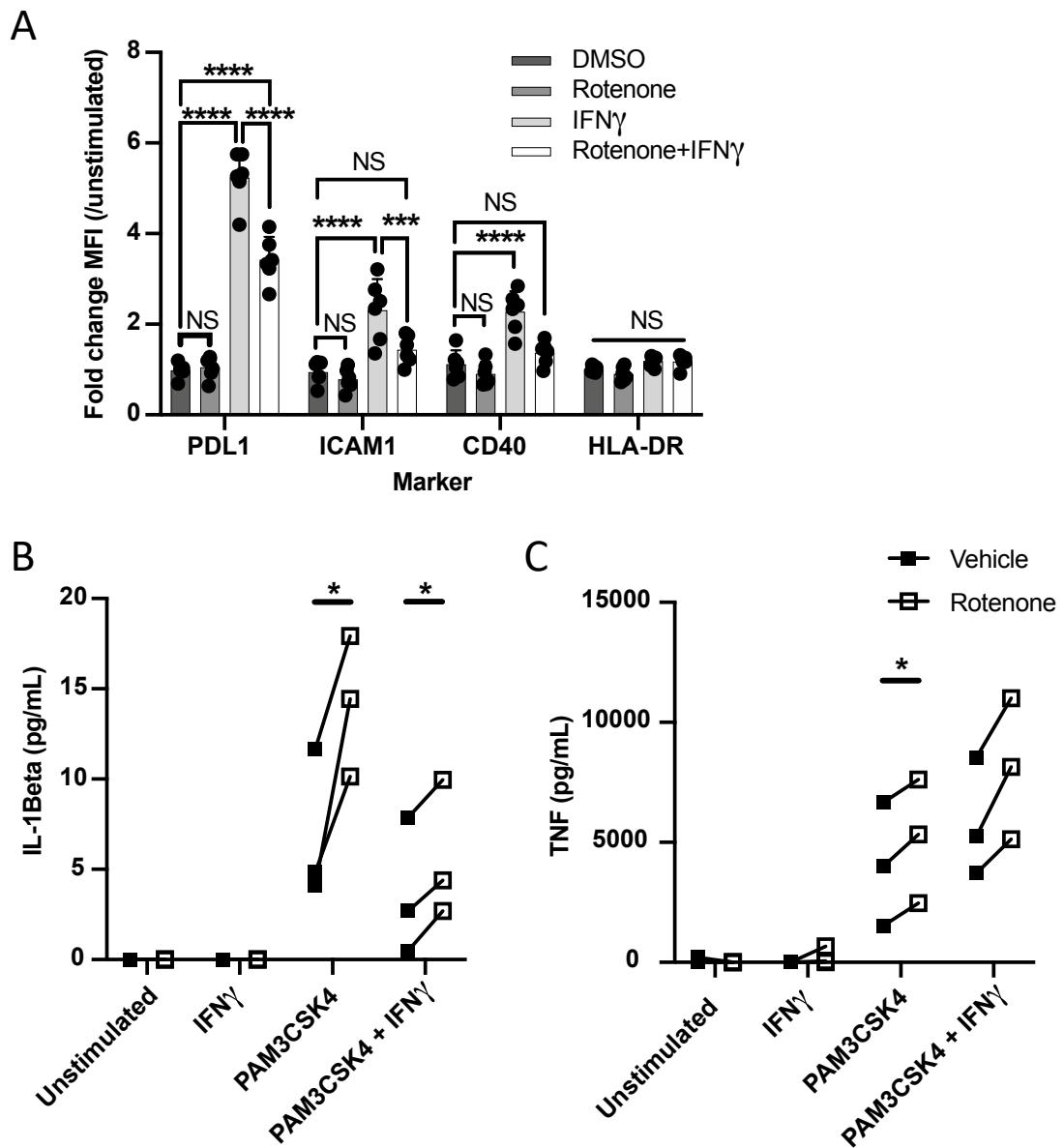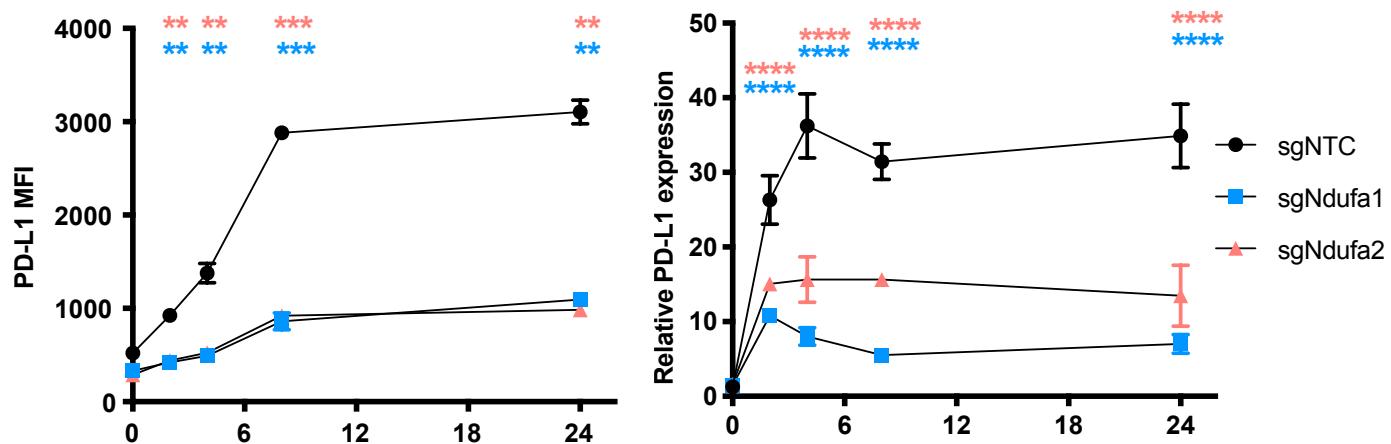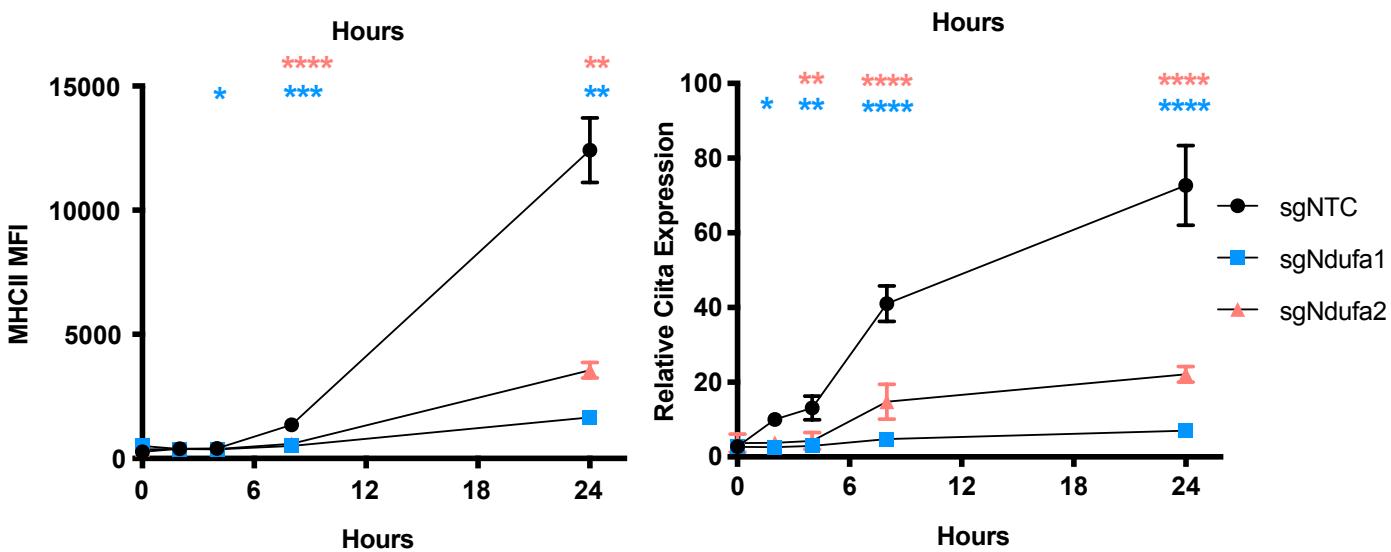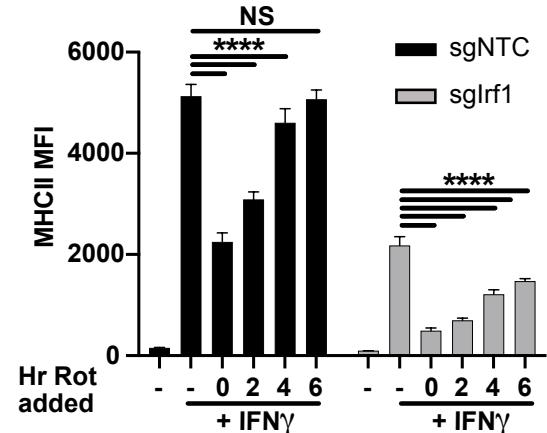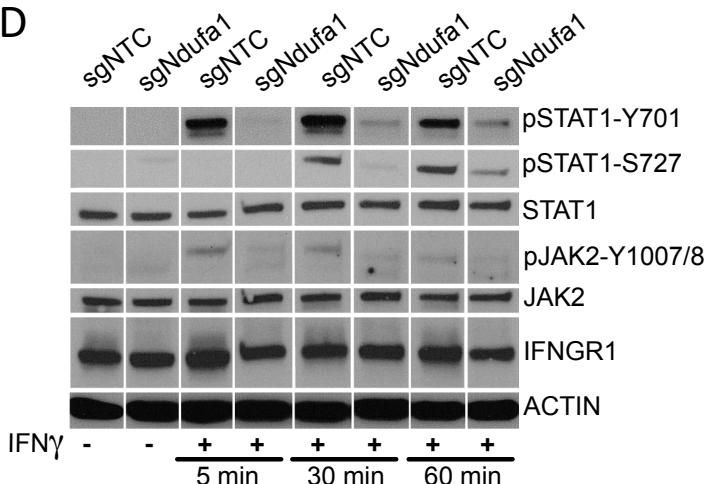
Figure 5
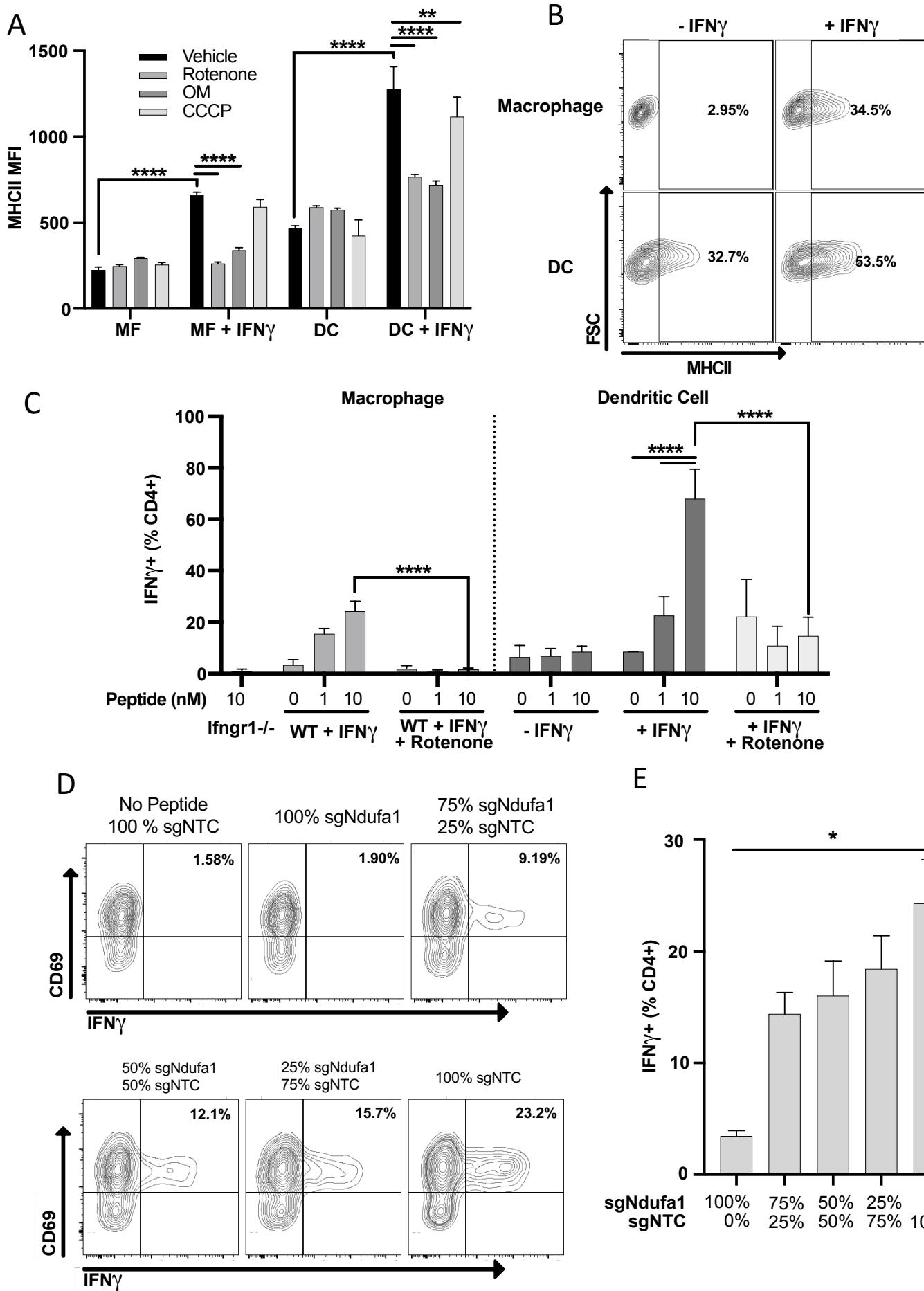
Figure 6

Figure 7

Supplemental Figure 1

Supplemental Figure 2